Fig. 23.14.3 Woodward-Lawson-Butler beams for $N = 8$.

Then, choose \tilde{n} such that $\tilde{n} \leq N/2$ and define an N -element array by its $N - 1$ zeros:

$$u_n = \begin{cases} \sigma\sqrt{B^2 + n^2}, & \text{for } 1 \leq n \leq \tilde{n} - 1 \\ n, & \text{for } \tilde{n} \leq n \leq N - \tilde{n} \\ -\sigma\sqrt{B^2 + (N - n)^2}, & \text{for } N - \tilde{n} + 1 \leq n \leq N - 1 \end{cases} \quad (23.15.1)$$

Fix the parameter σ such that $\sigma\sqrt{B^2 + \tilde{n}^2} = \tilde{n}$. Then, define the array polynomial:

$$A(z) = \prod_{n=1}^{N-1} (z - z_n), \quad \psi_n = \frac{2\pi u_n}{N}, \quad z_n = e^{j\psi_n}, \quad n = 1, 2, \dots, N - 1 \quad (23.15.2)$$

Write a MATLAB function that implements this procedure, and takes as input the parameters N, R, \tilde{n} and outputs the array weights and 3-dB width.

Apply your function to the following example $N = 21, R = 30$ dB, $\tilde{n} = 5$, with half-wavelength spacing $d = \lambda/2$. You will notice that, like the prolate array, the mainlobe is slightly narrower and the sidelobe level slightly better matched than the Taylor-Kaiser array. On the same graph, plot the array patterns $|A(\psi)|$ in dB for the present design, the Taylor Kaiser and the prolate arrays designed with the same specifications. Vary \tilde{n} to understand its effect on the design.

- 23.2 *Computer Experiment—Villeneuve array design.* Redesign the examples shown in Fig. 23.12.1 using Villeneuve's array design method and plot the array responses together with those of that figure. Vary the parameters N, R, \tilde{n} and compare the range of similarity of the Villeneuve versus the Taylor \tilde{n} method.

Currents on Linear Antennas

24.1 Hallén and Pocklington Integral Equations

In Sec. 15.4, we determined the electromagnetic fields generated by a given current distribution on a thin linear antenna, but did not discuss the mechanism by which the current distribution is set up and maintained. In Chap. 17, we assumed that the currents were sinusoidal, but this was only an approximation. Here, we discuss the integral equations that determine the exact form of the currents.

An antenna, whether transmitting or receiving, is always driven by an external source field. In transmitting mode, the antenna is driven by a generator voltage applied to its input terminals, and in receiving mode, by an incident electric field (typically, a uniform plane wave if it is arriving from far distances.) In either case, we will refer to this external source field as the “incident” field E_{in} .

The incident field E_{in} induces a current on the antenna. In turn, the current generates its own field E , which is radiated away. The total electric field is the sum $E_{\text{tot}} = E + E_{\text{in}}$. Assuming a perfectly conducting antenna, the *boundary conditions* are that the tangential components of the total electric field vanish on the antenna surface. These boundary conditions are enough to determine the current distribution induced on the antenna.

Fig. 24.1.1 depicts a z -directed thin cylindrical antenna of length l and radius a , with a current distribution $I(z)$ along its length. We will concentrate only on the z -component E_z of the electric field generated by the current and use cylindrical coordinates.

For a perfectly conducting antenna, the current is essentially a surface current at radial distance $\rho = a$ with surface density $J_s(z) = \hat{z}I(z)/2\pi a$, where in the “thin-wire approximation,” we may assume that the density is azimuthally symmetric with no dependence on the azimuthal angle ϕ . The corresponding volume current density will be as in Eq. (15.4.2):

$$J(\mathbf{r}) = J_s(z) \delta(\rho - a) = \hat{z}I(z) \delta(\rho - a) \frac{1}{2\pi a} \equiv \hat{z}J_z(\mathbf{r})$$

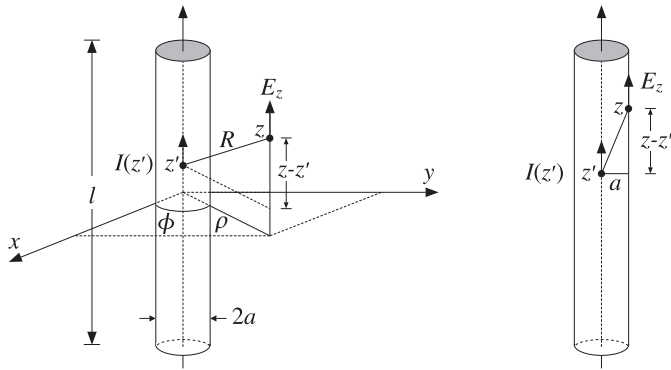


Fig. 24.1.1 Thin-wire model of cylindrical antenna.

Following the procedure of Sec. 15.4, we obtain the z-component of the vector potential:

$$A_z(z, \rho, \phi) = \frac{\mu}{4\pi} \int_{V'} \frac{J_z(\mathbf{r}') e^{-jkR}}{R} d^3\mathbf{r}' = \frac{\mu}{4\pi} \int_{V'} \frac{I(z') \delta(\rho' - a) e^{-jkR}}{2\pi a R} \rho' d\rho' d\phi' dz'$$

$$= \frac{\mu}{4\pi} \int_{-l/2}^{l/2} \int_0^{2\pi} \frac{I(z') e^{-jkR}}{2\pi R} d\phi' dz'$$

where $R = |\mathbf{r} - \mathbf{r}'| = \sqrt{(z - z')^2 + |\boldsymbol{\rho} - \boldsymbol{\rho}'|^2}$. Because $\rho' = a$, we have:

$$|\boldsymbol{\rho} - \boldsymbol{\rho}'|^2 = \rho^2 + a^2 - 2\boldsymbol{\rho} \cdot \boldsymbol{\rho}' = \rho^2 + a^2 - 2\rho a \cos(\phi' - \phi)$$

and because ϕ' appears only through the difference $\phi' - \phi$, we may change the variable of integration from ϕ' to $\phi' - \phi$. This implies that A_z will be cylindrically symmetric, that is, independent of ϕ . It follows that:

$$A_z(z, \rho) = \frac{\mu}{4\pi} \int_{-l/2}^{l/2} I(z') G(z - z', \rho) dz' \tag{24.1.1}$$

where we defined the *exact thin-wire kernel*:

$$G(z - z', \rho) = \frac{1}{2\pi} \int_0^{2\pi} \frac{e^{-jkR}}{R} d\phi' \tag{24.1.2}$$

with $R = \sqrt{(z - z')^2 + \rho^2 + a^2 - 2\rho a \cos \phi'}$. In the limit of a thin antenna, $a \rightarrow 0$, Eq. (24.1.1) reduces to:

$$A_z(z, \rho) = \frac{\mu}{4\pi} \int_{-l/2}^{l/2} I(z') G_{\text{app}}(z - z', \rho) dz' \tag{24.1.3}$$

where $G_{\text{app}}(z - z', \rho)$ is the *approximate* or *reduced thin-wire kernel*:

$$G_{\text{app}}(z - z', \rho) = \frac{e^{-jkR}}{R} \tag{24.1.4}$$

with $R = \sqrt{(z - z')^2 + \rho^2}$. Eq. (24.1.3) is the same as (15.4.3) because the limit $a = 0$ is equivalent to assuming that the current density is a line current $\mathbf{J}(\mathbf{r}) = \hat{\mathbf{z}} I(z) \delta(x) \delta(y)$, as given by Eq. (15.4.1).

Given the vector potential $A_z(z, \rho)$, the z-component of the electric field generated by the current is obtained from Eq. (15.4.6):

$$j\omega\mu\epsilon E_z(z, \rho) = (\partial_z^2 + k^2) A_z(z, \rho) \tag{24.1.5}$$

The values of the vector potential A_z and the electric field E_z on the surface of the wire antenna are obtained by setting $\rho = a$:

$$A_z(z, a) = \frac{\mu}{4\pi} \int_{-l/2}^{l/2} I(z') G(z - z', a) dz' \tag{24.1.6}$$

To simplify the notation, we will denote $A_z(z, a)$ and $G(z - z', a)$ by $A_z(z)$ and $G(z - z')$. The boundary condition on the surface is that the z-component of the total electric field vanish, that is, at $\rho = a$:

$$E_{z,\text{tot}}(z, a) = E_z(z, a) + E_{z,\text{in}}(z, a) = 0$$

Thus, with $E_z(z) = E_z(z, a)$ and $E_{\text{in}}(z) = E_{z,\text{in}}(z, a)$, we have $E_z(z) = -E_{\text{in}}(z)$, and Eq. (24.1.5) can be expressed in terms of the z-component of the incident field:

$$(\partial_z^2 + k^2) A_z(z) = -j\omega\mu\epsilon E_{\text{in}}(z) \tag{24.1.7}$$

Either kernel can be used in Eq. (24.1.6). If the approximate kernel $G_{\text{app}}(z)$ is used, then it is still meaningful to consider the boundary conditions at the cylindrical surface (i.e., at $\rho = a$) of the antenna, as shown on the right of Fig. 24.1.1.

To summarize, given an incident field $E_{\text{in}}(z)$ that is known along the length of the antenna, Eq. (24.1.7) may be solved for $A_z(z)$ and then the integral equation (24.1.6) can be solved for the current $I(z)$.

Depending on how this procedure is carried out, one obtains either the Hallén or the Pocklington equations. Solving Eq. (24.1.7) by formally inverting the differential operator $(\partial_z^2 + k^2)$ and combining with (24.1.6), we obtain *Hallén's integral equation*:

$$\frac{\mu}{4\pi} \int_{-l/2}^{l/2} I(z') G(z - z') dz' = -j\omega\mu\epsilon (\partial_z^2 + k^2)^{-1} E_{\text{in}}(z) \tag{Hallén} \tag{24.1.8}$$

Alternatively, applying the differential operator $(\partial_z^2 + k^2)$ directly to Eq. (24.1.6) and combining with (24.1.7), we obtain *Pocklington's integral equation*:

$$\frac{\mu}{4\pi} \int_{-l/2}^{l/2} I(z') (\partial_z^2 + k^2) G(z - z') dz' = -j\omega\mu\epsilon E_{\text{in}}(z) \tag{Pocklington} \tag{24.1.9}$$

The two integral equations must be solved subject to the constraint that the current $I(z)$ vanish at the antenna ends, that is, $I(l/2) = I(-l/2) = 0$. The exact and approximate kernels evaluated on the antenna surface are:

$$G(z - z') = \frac{1}{2\pi} \int_0^{2\pi} \frac{e^{-jkR}}{R} d\phi', \quad R = \sqrt{(z - z')^2 + 2a^2 - 2a^2 \cos \phi'} \tag{24.1.10}$$

$$G_{\text{app}}(z - z') = \frac{e^{-jkR}}{R}, \quad R = \sqrt{(z - z')^2 + a^2}$$

The inverse differential operator in the right-hand side of Eq. (24.1.8) can be rewritten as an integral convolutional operator acting on E_{in} . We discuss this in detail in Sec. 24.3. We will then consider the numerical solutions of these equations using either the exact or the approximate kernels. The numerical evaluation of these kernels is discussed in Sec. 24.7.

24.2 Delta-Gap, Frill Generator, and Plane-Wave Sources

Although the external source field $E_{in}(z)$ can be specified arbitrarily, there are two special cases of practical importance. One is the so-called delta-gap model, which imitates the way a transmitting antenna is fed by a transmission line. The other is a uniform plane wave incident at an angle on a receiving antenna connected to a load impedance. Fig. 24.2.1 depicts these cases.

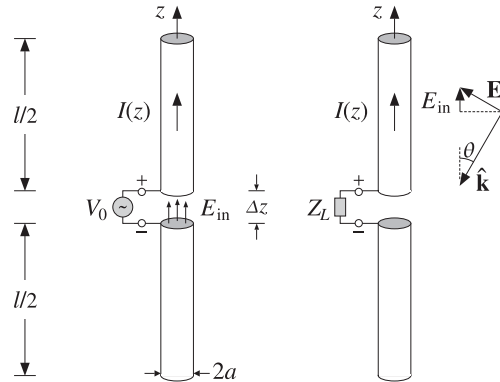


Fig. 24.2.1 External sources acting on a linear antenna.

The left figure shows the *delta-gap* model of a generator voltage applied between the upper and lower halves of the antenna across a short gap of length Δz . The applied voltage V_0 can be thought of as arising from an electric field—the “incident” field in this case—which exists only within the gap, such that

$$V_0 = \int_{-\Delta z/2}^{\Delta z/2} E_{in}(z) dz \tag{24.2.1}$$

A simplified case arises when we take the limit $\Delta z \rightarrow 0$. Then, approximately, $V_0 = E_{in}\Delta z$, or $E_{in} = V_0/\Delta z$. In order to maintain a finite value of V_0 in the left-hand side of Eq. (24.2.1), E_{in} must become commensurately large. This means that in this limit,

$$E_{in}(z) = V_0\delta(z) \tag{delta-gap model of incident field} \tag{24.2.2}$$

King [3] has discussed the case of a finite Δz . An alternative type of excitation input is the *frill generator* [6,7] defined by:

$$E_{in}(z) = \frac{V_0}{2 \ln(b/a)} \left[\frac{e^{-jkR_a}}{R_a} - \frac{e^{-jkR_b}}{R_b} \right], \quad \begin{matrix} R_a = \sqrt{z^2 + a^2} \\ R_b = \sqrt{z^2 + b^2} \end{matrix} \tag{24.2.3}$$

where $b > a$. The case of a receiving antenna with a uniform plane wave incident at a polar angle θ and such that the propagation vector \hat{k} is co-planar with the antenna axis is shown on the right of Fig. 24.2.1.

The electric field vector is perpendicular to \hat{k} and has a space dependence $E_0 e^{-jk \cdot r}$. For a thin antenna, we may evaluate the field along the z -axis, that is, we set $x = y = 0$ so that $e^{-jk \cdot r} = e^{-jk_z z} = e^{jk_z \cos \theta}$ because $k_z = -k \cos \theta$. Then, the z -component of the incident field will be:

$$E_{in}(z) = E_0 \sin \theta e^{jk_z \cos \theta} \tag{incident uniform plane wave} \tag{24.2.4}$$

If the wave is incident from broadside ($\theta = \pi/2$), then $E_{in}(z) = E_0$, that is, a constant along the antenna length. And, if $\theta = 0$ or π , then $E_{in}(z) = 0$.

24.3 Solving Hallén's Equation

Instead of working with the vector potential $A_z(z)$ it proves convenient to work with a scaled version of it that has units of volts and is defined as:

$$V(z) = 2jcA_z(z) \tag{24.3.1}$$

where c is the speed of light. We note that $V(z)$ is not the scalar potential $\varphi(z)$ along the antenna length. From the Lorenz condition, Eq. (15.4.5), we have $\partial_z A_z = -j\omega\mu\epsilon\varphi(z)$. Multiplying by $2jc$ and noting that $c\omega\epsilon\mu = \omega/c = k$, we find:

$$\partial_z V(z) = 2k\varphi(z) \tag{24.3.2}$$

Multiplying both sides of Eq. (24.1.7) by $2jc$, we can rewrite it as:

$$(\partial_z^2 + k^2)V(z) = 2kE_{in}(z) \tag{24.3.3}$$

Similarly, Eq. (24.1.6) becomes:

$$\frac{j\eta}{2\pi} \int_{-h}^h G(z-z')I(z') dz' = V(z) \tag{24.3.4}$$

where $\eta = \sqrt{\mu/\epsilon}$, and for later convenience, we introduced the half-length $h = l/2$ of the antenna. Eqs. (24.3.3)-(24.3.4) represent our rescaled version of Hallén's equations.

Formally, we can write $V(z) = 2k(\partial_z^2 + k^2)^{-1}E_{in}(z)$, but we prefer to express $V(z)$ as an integral operator acting on $E_{in}(z)$. A particular solution of (24.3.3) is obtained with the help of the Green's function $F(z)$ for this differential equation:

$$(\partial_z^2 + k^2)F(z) = 2k\delta(z) \tag{24.3.5}$$

The general solution of Eq. (24.3.3) is obtained by adding the most general solution of the homogeneous equation, $(\partial_z^2 + k^2)V(z) = 0$, to the Green's function solution:

$$V(z) = C_1 e^{jkz} + C_2 e^{-jkz} + \int_{-h}^h F(z-z') E_{in}(z') dz' \quad (24.3.6)$$

With a re-definition of the constants C_1, C_2 , we can also write:

$$V(z) = C_1 \cos kz + C_2 \sin kz + \int_{-h}^h F(z-z') E_{in}(z') dz' \quad (24.3.7)$$

In fact, $F(z)$ itself is defined up to an arbitrary solution of the homogeneous equation. If $F(z)$ satisfies Eq. (24.3.5), so does $F_1(z) = F(z) + C_1 e^{jkz} + C_2 e^{-jkz}$, with arbitrary constants C_1, C_2 . Some possible choices for $F(z)$ are as follows. They differ from each other by a homogeneous term:

$F_1(z) = j e^{-jk z } = F_2(z) + j \cos kz$	(24.3.8)
$F_2(z) = \sin k z = F_3(z) - \sin kz$	
$F_3(z) = 2 \sin(kz) u(z) = F_4(z) + 2 \sin kz$	
$F_4(z) = -2 \sin(kz) u(-z)$	

where $u(z)$ is the unit-step function. All satisfy Eq. (24.3.5) as well as the required discontinuity conditions on their first derivative, that is,

$$F'(0+) - F'(0-) = 2k \quad (24.3.9)$$

This discontinuity condition is obtained by integrating Eq. (24.3.5) over the small interval $-\epsilon \leq z \leq \epsilon$ and then taking the limit $\epsilon \rightarrow 0$ and assuming that $F(z)$ itself is continuous at $z = 0$. Depending on the choice of $F(z)$, the corresponding solution $V(z)$ of Eq. (24.3.3) can be written in the equivalent forms (each with different C_1, C_2):

$$\begin{aligned} V(z) &= C_1 e^{jkz} + C_2 e^{-jkz} + \int_{-h}^h j e^{-jk|z-z'|} E_{in}(z') dz' \\ V(z) &= C_1 e^{jkz} + C_2 e^{-jkz} + \int_{-h}^h \sin(k|z-z'|) E_{in}(z') dz' \\ V(z) &= C_1 e^{jkz} + C_2 e^{-jkz} + 2 \int_{-h}^z \sin(k(z-z')) E_{in}(z') dz' \\ V(z) &= C_1 e^{jkz} + C_2 e^{-jkz} - 2 \int_z^h \sin(k(z-z')) E_{in}(z') dz' \end{aligned} \quad (24.3.10)$$

We will use mostly the first and second choices for $F(z)$, that is, $F(z) = j e^{-jk|z|}$ and $F(z) = \sin k|z|$. Combining the solution for $V(z)$ with Eq. (24.3.4), we obtain the equivalent form of Hallén's integral equation for an arbitrary incident field:

$$\frac{j\eta}{2\pi} \int_{-h}^h G(z-z') I(z') dz' = C_1 e^{jkz} + C_2 e^{-jkz} + \int_{-h}^h F(z-z') E_{in}(z') dz' \quad (24.3.11)$$

or, alternatively,

$$\frac{j\eta}{2\pi} \int_{-h}^h G(z-z') I(z') dz' = C_1 \cos kz + C_2 \sin kz + \int_{-h}^h F(z-z') E_{in}(z') dz'$$

The constants C_1, C_2 are determined from the end conditions $I(h) = I(-h) = 0$. Next, we consider the particular forms of Eq. (24.3.11) in the delta-gap and plane-wave cases. In the delta-gap case, we have $E_{in}(z) = V_0 \delta(z)$ and the integral on the right-hand side can be done trivially, giving:

$$\int_{-h}^h F(z-z') E_{in}(z') dz' = \int_{-h}^h F(z-z') V_0 \delta(z') dz' = V_0 F(z)$$

Thus, we have the integral equation:

$$\frac{j\eta}{2\pi} \int_{-h}^h G(z-z') I(z') dz' = C_1 \cos kz + C_2 \sin kz + V_0 F(z)$$

We expect the current $I(z)$ to be an even function of z (because $E_{in}(z)$ is), and thus we may drop the C_2 term. Using $F(z) = \sin k|z|$ as our Green's function choice, we obtain Hallén's equation for the delta-gap case:

$$\frac{j\eta}{2\pi} \int_{-h}^h G(z-z') I(z') dz' = V(z) = C_1 \cos kz + V_0 \sin k|z| \quad (24.3.12)$$

This equation forms the basis for determining the current on a center-driven linear antenna. We will consider several approximate solutions of it as well as numerical solutions based on moment methods.

We can verify that $V(z)$ correctly gives the potential difference between the upper and lower halves of the antenna. Differentiating $V(z)$ about $z = 0$ and using Eq. (24.3.2), we have:

$$V'(0+) - V'(0-) = 2kV_0 = 2k(\varphi(0+) - \varphi(0-)) \Rightarrow \varphi(0+) - \varphi(0-) = V_0$$

As a second example, consider the case of an antenna receiving a uniform plane wave with incident field as in Eq. (24.2.4). Using $F(z) = j e^{-jk|z|}$ as the Green's function, the convolution integral of $F(z)$ and $E_{in}(z)$ can be done easily giving:

$$\int_{-h}^h j e^{-jk|z-z'|} E_0 \sin \theta e^{jkz' \cos \theta} dz' = \frac{2E_0}{k \sin \theta} e^{jkz \cos \theta} + (\text{homogeneous terms})$$

where the last terms are solutions of the homogeneous equation, and thus, can be absorbed into the other homogeneous terms of $V(z)$. Because the current is not expected to be symmetric in z , we must keep both homogeneous terms, resulting in Hallén's equation for a receiving antenna:

$$\frac{j\eta}{2\pi} \int_{-h}^h G(z-z') I(z') dz' = V(z) = C_1 e^{jkz} + C_2 e^{-jkz} + \frac{2E_0}{k \sin \theta} e^{jkz \cos \theta} \quad (24.3.13)$$

24.4 Sinusoidal Current Approximation

Here, we look at simplified solutions of Eq. (24.3.12), which justify the common sinusoidal assumption for the current. We work with the approximate kernel.

Inspecting the quantity $G_{\text{app}}(z - z') = e^{-jkR}/R$ in the integral equation (24.3.12), we note that as the integration variable z' sweeps past z , the denominator becomes very large, because $R = a$ at $z' = z$. Therefore, the integral is dominated by the value of the integrand near $z' = z$. We can write approximately,

$$\frac{j\eta}{2\pi} \int_{-h}^h G_{\text{app}}(z - z') I(z') dz' \approx \bar{Z}(z) I(z) \approx \tilde{Z} I(z) \tag{24.4.1}$$

where $\tilde{Z}(z)$ is a sort of an average value of $j\eta G_{\text{app}}(z - z')/2\pi$ in the neighborhood of $z' = z$. This quantity varies slowly with z and we may approximate it with a constant, say \bar{Z} . Then, Hallén's equation (24.3.12) becomes approximately:

$$\tilde{Z} I(z) = V(z) = C_1 \cos kz + V_0 \sin k|z|$$

This shows that $I(z)$ is approximately sinusoidal. The constant C_1 is fixed by the end-condition $I(h) = 0$, which gives:

$$C_1 \cos kh + V_0 \sin kh = 0 \Rightarrow C_1 = -V_0 \frac{\sin kh}{\cos kh}$$

so that $I(z)$ becomes:

$$\tilde{Z} I(z) = -V_0 \frac{1}{\cos kh} [\sin kh \cos kz - \cos kh \sin k|z|] = -V_0 \frac{1}{\cos kh} \sin(k(h - |z|))$$

Solving for $I(z)$, we obtain the common standing-wave expression for the current:

$$I(z) = I(0) \frac{\sin(k(h - |z|))}{\sin kh}, \quad I(0) = -\frac{V_0 \sin kh}{\bar{Z} \cos kh} \tag{24.4.2}$$

where $I(0)$ is the input current at $z = 0$. The crude approximation of Eq. (24.4.1) can be refined further using King's three-term approximation discussed in Sec. 24.6. From Eq. (24.4.2), the antenna input impedance is seen to be:

$$Z_A = \frac{V_0}{I(0)} = -\bar{Z} \cot kh \tag{24.4.3}$$

24.5 Reflecting and Center-Loaded Receiving Antennas

A similar approximation to Hallén's equation can be carried out in the plane-wave case shown in Fig. 24.2.1. We distinguish three cases: (a) $Z_L = 0$, corresponding to a reflecting parasitic antenna with short-circuited output terminals, (b) $Z_L = \infty$, corresponding to open-circuited terminals, and (c) arbitrary Z_L , corresponding to a center-loaded receiving antenna. See Ref. [12] for more details on this approach.

By finding the short-circuit current from case (a) and the open-circuit voltage from case (b), we will determine the output impedance of the receiving antenna, that is, the

Thevenin impedance Z_A of the model of Sec. 16.4, and show that it is equal to the input impedance (24.4.3) of the transmitting antenna, in accordance with the reciprocity principle. We will also show from case (c) that the angular gain pattern of the receiving antenna agrees with that of the transmitting one.

Starting with the short-circuited case, the approximation of Eq. (24.4.1) applied to (24.3.13) gives:

$$\tilde{Z} I(z) = V(z) = C_1 e^{jkz} + C_2 e^{-jkz} + \frac{2E_0}{k \sin \theta} e^{jkz \cos \theta}$$

The end-point conditions $I(h) = I(-h) = 0$ provide two equations in the two unknowns C_1, C_2 , that is,

$$C_1 e^{jkh} + C_2 e^{-jkh} + \frac{2E_0}{k \sin \theta} e^{jkh \cos \theta} = 0$$

$$C_1 e^{-jkh} + C_2 e^{jkh} + \frac{2E_0}{k \sin \theta} e^{-jkh \cos \theta} = 0$$

with solution:

$$C_1 = -\frac{E_0 \sin(kh(1 + \cos \theta))}{k \sin \theta \sin kh \cos kh}, \quad C_2 = -\frac{E_0 \sin(kh(1 - \cos \theta))}{k \sin \theta \sin kh \cos kh}$$

Then, the current $I(z)$ becomes:

$$I(z) = \frac{1}{\bar{Z}} [C_1 e^{jkz} + C_2 e^{-jkz} + \frac{2E_0}{k \sin \theta} e^{jkz \cos \theta}] \tag{24.5.1}$$

For normal incidence, $\theta = 90^\circ$, we have $C_1 = C_2$ and Eq. (24.5.1) becomes:

$$I(z) = \frac{2E_0}{\bar{Z} k \cos kh} (\cos kh - \cos kz) \tag{24.5.2}$$

For $\theta = 0$ and $\theta = \pi$, the z -component of the incident field is zero, $E_{\text{in}}(z) = 0$, and we expect $I(z) = 0$. This can be verified by carefully taking the limit of Eq. (24.5.1) at $\theta = 0, \pi$, with the seemingly diverging term $2E_0/k \sin \theta$ getting canceled.

The short-circuit current at the output terminals is obtained by setting $z = 0$ in Eq. (24.5.1):

$$I_{\text{sc}} = I(0) = \frac{1}{\bar{Z}} [C_1 + C_2 + \frac{2E_0}{k \sin \theta}]$$

Inserting the expressions for C_1, C_2 , we find:

$$I_{\text{sc}} = \frac{2E_0}{\bar{Z} k \cos kh} \frac{\cos kh - \cos(kh \cos \theta)}{\sin \theta} \tag{24.5.3}$$

For the open-circuit case, the incident field will induce an open-circuit voltage across the gap, and therefore, the scalar potential $\varphi(z)$ will be discontinuous at $z = 0$. In addition, the current must vanish at $z = 0$. Therefore, we must apply Eq. (24.3.13) separately to the upper and lower halves of the antenna. Using $\cos kz$ and $\sin kz$ as the homogeneous terms, instead of $e^{\pm jkz}$, we have the approximation:

$$\tilde{Z} I(z) = V(z) = \begin{cases} C_1 \cos kz + C_2 \sin kz + \frac{2E_0}{k \sin \theta} e^{jkz \cos \theta}, & z \geq 0 \\ D_1 \cos kz + D_2 \sin kz + \frac{2E_0}{k \sin \theta} e^{jkz \cos \theta}, & z \leq 0 \end{cases}$$

The conditions $I(0+) = I(h) = 0$ and $I(0-) = I(-h) = 0$ provide four equations in the four unknowns C_1, C_2, D_1, D_2 . They are:

$$\begin{aligned} C_1 + \frac{2E_0}{k \sin \theta} &= 0, & C_1 \cos kh + C_2 \sin kh + \frac{2E_0}{k \sin \theta} e^{jkh \cos \theta} &= 0 \\ D_1 + \frac{2E_0}{k \sin \theta} &= 0, & D_1 \cos kh - D_2 \sin kh + \frac{2E_0}{k \sin \theta} e^{-jkh \cos \theta} &= 0 \end{aligned}$$

with solution:

$$\begin{aligned} C_1 = D_1 &= -\frac{2E_0}{k \sin \theta} \\ C_2 &= \frac{2E_0(\cos kh - e^{jkh \cos \theta})}{k \sin \theta \sin kh}, & D_2 &= -\frac{2E_0(\cos kh - e^{-jkh \cos \theta})}{k \sin \theta \sin kh} \end{aligned}$$

The open-circuit voltage is $V_{oc} = \varphi(0+) - \varphi(0-)$. Using Eq. (24.3.2), we have:

$$V'(0+) - V'(0-) = 2kV_{oc} = k(C_2 - D_2) \quad \Rightarrow \quad V_{oc} = \frac{1}{2}(C_2 - D_2)$$

and using the solution for C_2, D_2 , we find:

$$V_{oc} = \frac{2E_0}{k \sin kh} \frac{\cos kh - \cos(kh \cos \theta)}{\sin \theta} \quad (24.5.4)$$

Having found the short-circuit current and open-circuit voltage, we obtain the corresponding output Thévenin impedance by dividing Eq. (24.5.4) and (24.5.3):

$$Z_A = -\frac{V_{oc}}{I_{sc}} = -\bar{Z} \cot kh \quad (24.5.5)$$

where the minus sign is due to the fact that I_{sc} is flowing into (instead of out of) the top antenna terminal. We note that Eq. (24.5.5) agrees with (24.4.3) of the transmitting case.

Equations (24.5.3) and (24.5.4) are special cases of a more general result, which is a consequence of the reciprocity principle (for example, see [34]). Given an incident field on a receiving linear antenna, the induced short-circuit current and open-circuit voltage at its terminals are given by:

$$\boxed{I_{sc} = \frac{1}{V_0} \int_{-h}^h E_{in}(z) I(z) dz, \quad V_{oc} = -\frac{1}{I_0} \int_{-h}^h E_{in}(z) I(z) dz} \quad (24.5.6)$$

where $I(z)$ is the current generated by V_0 when the antenna is transmitting. Inserting Eq. (24.4.2) into (24.5.6), we can easily derive Eqs. (24.5.3) and (24.5.4). We will use (24.5.6) in Sec. 25.3 to derive the mutual impedance between two antennas.

Finally, we consider case (c) of an arbitrary load impedance Z_L . The current will be continuous across the gap but it does not have to vanish at $z = 0$. The voltage difference across the gap will be equal to the voltage drop across the load, that is, $V_L = -Z_L I(0)$. The approximate Hallén equation is now:

$$\bar{Z} I(z) = V(z) = \begin{cases} C_1 \cos kz + C_2 \sin kz + \frac{2E_0}{k \sin \theta} e^{jkz \cos \theta}, & z \geq 0 \\ D_1 \cos kz + D_2 \sin kz + \frac{2E_0}{k \sin \theta} e^{jkz \cos \theta}, & z \leq 0 \end{cases}$$

where $D_1 = C_1$ because of the continuity of $I(z)$ at $z = 0$. The end conditions, $I(h) = I(-h) = 0$, give:

$$\begin{aligned} C_1 \cos kh + C_2 \sin kh + \frac{2E_0}{k \sin \theta} e^{jkh \cos \theta} &= 0 \\ C_1 \cos kh - D_2 \sin kh + \frac{2E_0}{k \sin \theta} e^{-jkh \cos \theta} &= 0 \end{aligned}$$

Moreover, we have the discontinuity condition:

$$V'(0+) - V'(0-) = 2kV_L = k(C_2 - D_2) \quad \Rightarrow \quad V_L = \frac{1}{2}(C_2 - D_2)$$

Ohm's law at the load gives:

$$V_L = -Z_L I(0) = -\frac{Z_L}{\bar{Z}} \left(C_1 + \frac{2E_0}{k \sin \theta} \right) = \frac{Z_L}{Z_A} \left(C_1 + \frac{2E_0}{k \sin \theta} \right) \cot kh$$

where we used Eq. (24.5.5). Solving the above four equations for C_1, C_2, D_2, V_L , we find eventually:

$$V_L = \frac{Z_L}{Z_A + Z_L} \frac{2E_0}{k \sin kh} \frac{\cos kh - \cos(kh \cos \theta)}{\sin \theta} = \frac{V_{oc} Z_L}{Z_A + Z_L} \quad (24.5.7)$$

This is equivalent to the Thévenin model that we used in Sec. 16.4. The power delivered to the load will be proportional to $|V_L|^2$, which is proportional to the gain pattern of a transmitting dipole, that is,

$$\left| \frac{\cos kh - \cos(kh \cos \theta)}{\sin \theta} \right|^2$$

24.6 King's Three-Term Approximation

To improve the crude sinusoidal approximation of Eq. (24.4.1), we must look more carefully at the properties of the kernel. Separating its real and imaginary parts, we have:

$$\frac{j\eta}{2\pi} G_{app}(z - z') = \frac{j\eta}{2\pi} \frac{e^{-jkR}}{R} = \frac{k\eta}{2\pi} \left[\frac{\sin kR}{kR} + j \frac{\cos kR}{kR} \right]$$

For R near zero, the imaginary part becomes very large and we may apply the approximation (24.4.1) to it. But, the real part remains finite at $R = 0$. For $kR \leq \pi$, which will be guaranteed if $kh \leq \pi$, the sinc function can be very well approximated by $\cos(kR/2) \approx \cos(k|z - z'|/2)$ as can be verified by plotting the two functions. Therefore,

$$\frac{\sin kR}{kR} \approx \cos(kR/2) \approx \cos(k(z - z')/2), \quad \text{for } kR \leq \pi \quad (24.6.1)$$

Using this approximation for the real part of the kernel, and applying the approximation of Eq. (24.4.1) to its imaginary part, King has shown [4,94] that an improved approximation of the convolution integral is as follows:

$$\frac{j\eta}{2\pi} \int_{-h}^h G_{app}(z - z') I(z') dz' \approx R \cos\left(\frac{kz}{2}\right) + jXI(z) \quad (24.6.2)$$

where R, X are appropriate constants, which are real if $I(z)$ is real. The approximation also assumes that the current is symmetric, $I(z) = I(-z)$. Indeed, we have:

$$\begin{aligned} \frac{j\eta}{2\pi} \int_{-h}^h G_{\text{app}}(z-z')I(z')dz' &= \frac{k\eta}{2\pi} \int_{-h}^h \left[\cos\left(\frac{k(z-z')}{2}\right) + j\frac{\cos kR}{kR} \right] I(z')dz' \\ &= \frac{k\eta}{2\pi} \int_{-h}^h \left[\cos\left(\frac{kz}{2}\right)\cos\left(\frac{kz'}{2}\right)I(z') + \sin\left(\frac{kz}{2}\right)\sin\left(\frac{kz'}{2}\right)I(z') + j\frac{\cos kR}{kR}I(z') \right] dz' \end{aligned}$$

The first term is of the form $R \cos(kz/2)$, the second term vanishes because of the assumed even symmetry of $I(z)$, and the third term is of the form $jXI(z)$. It follows that the Hallén equation (24.3.12) can be approximated by:

$$R \cos\left(\frac{kz}{2}\right) + jXI(z) = V(z) = C_1 \cos kz + V_0 \sin k|z|$$

This shows that the current $I(z)$ is a linear combination of the sinusoidal terms $\sin k|z|$, $\cos kz$, and $\cos(kz/2)$, and leads to King's three-term approximation for the current [4,94], which incorporates the condition $I(h) = 0$. There are two alternative forms:

$$I(z) = A_1 I_1(z) + A_2 I_2(z) + A_3 I_3(z) = A'_1 I'_1(z) + A'_2 I'_2(z) + A'_3 I'_3(z) \quad (24.6.3)$$

where the expansion currents are defined by:

$I_1(z) = \sin k z - \sin kh$,	$I'_1(z) = \sin(k(h - z))$,	$I'_2(z) = \cos kz - \cos kh$	(24.6.4)
$I_2(z) = \cos kz - \cos kh$		$I'_3(z) = \cos(kz/2) - \cos(kh/2)$			
$I_3(z) = \cos(kz/2) - \cos(kh/2)$					

Using the trigonometric identity $I_1(z) = I'_2(z) \tan kh - I'_1(z) / \cos kh$, the relationship between the primed and unprimed coefficients is:

$$\begin{bmatrix} A'_1 \\ A'_2 \end{bmatrix} = \frac{1}{\cos kh} \begin{bmatrix} -1 & 0 \\ \sin kh & \cos kh \end{bmatrix} \begin{bmatrix} A_1 \\ A_2 \end{bmatrix}, \quad A'_3 = A_3 \quad (24.6.5)$$

The condition number of the transformation matrix is $1/|\cos kh|$, and the transformation breaks down when $\cos kh = 0$, that is, when the antenna length $l = 2h$ is an odd-multiple of $\lambda/2$. In that case, only the unprimed form may be used. Otherwise, the primed form is preferable because the term $I'_1(z) = \sin(k(h - |z|))$ has the conventional standing-wave form. We will work with the unprimed form because it is always possible. The MATLAB function `kingprime` transforms the unprimed coefficients into the primed ones:

```
Aprime = kingprime(L,A); % converts from unprimed to primed form
```

To determine the expansion coefficients A_1, A_2, A_3 , we insert Eq. (24.6.3) into Hallén's equation (24.3.12) and get:

$$A_1 V_1(z) + A_2 V_2(z) + A_3 V_3(z) = V(z) = C_1 \cos kz + V_0 \sin k|z| \quad (24.6.6)$$

where

$$V_i(z) = \frac{j\eta}{2\pi} \int_{-h}^h G_{\text{app}}(z-z')I_i(z')dz', \quad i = 1, 2, 3 \quad (24.6.7)$$

At $z = h$, we have:

$$A_1 V_1(h) + A_2 V_2(h) + A_3 V_3(h) = V(h) = C_1 \cos kh + V_0 \sin kh \quad (24.6.8)$$

Subtracting Eqs. (24.6.6) and (24.6.8), and defining $V_{di}(z) = V_i(z) - V_i(h)$, we have:

$$A_1 V_{d1}(z) + A_2 V_{d2}(z) + A_3 V_{d3}(z) = C_1 (\cos kz - \cos kh) + V_0 (\sin k|z| - \sin kh)$$

Using the definition (24.6.4), we can write:

$$A_1 V_{d1}(z) + A_2 V_{d2}(z) + A_3 V_{d3}(z) = C_1 I_2(z) + V_0 I_1(z) \quad (24.6.9)$$

Introducing the difference kernel $G_d(z-z') = G_{\text{app}}(z-z') - G_{\text{app}}(h-z')$, we have:

$$V_{di}(z) = \frac{j\eta}{2\pi} \int_{-h}^h G_d(z-z')I_i(z')dz', \quad i = 1, 2, 3 \quad (24.6.10)$$

The improved approximation (24.6.2) applied to the difference kernel gives:

$$\frac{j\eta}{2\pi} \int_{-h}^h G_d(z-z')I(z')dz' = R(\cos(kz/2) - \cos(kh/2)) + jXI(z) = RI_3(z) + jXI(z)$$

Therefore, applying it to the three separate currents $I_1(z), I_2(z), I_3(z)$, we obtain:

$$V_{di}(z) = V_i(z) - V_i(h) = R_i I_3(z) + jX_i I_i(z), \quad i = 1, 2, 3 \quad (24.6.11)$$

Inserting these approximations in Eq. (24.6.6), we have:

$$\begin{aligned} A_1 [R_1 I_3(z) + jX_1 I_1(z)] + A_2 [R_2 I_3(z) + jX_2 I_2(z)] + A_3 [R_3 I_3(z) + jX_3 I_3(z)] &= \\ &= C_1 I_2(z) + V_0 I_1(z) \end{aligned}$$

Defining $Z_3 = R_3 + jX_3$ and matching the coefficients of $I_1(z), I_2(z), I_3(z)$ in the two sides, gives three equations in the four unknowns A_1, A_2, A_3, C_1 :

$$jX_1 A_1 = V_0, \quad jX_2 A_2 - C_1 = 0, \quad R_1 A_1 + R_2 A_2 + Z_3 A_3 = 0$$

The fourth equation is (24.6.8). Thus, we obtain the linear system:

$$\begin{bmatrix} jX_1 & 0 & 0 & 0 \\ 0 & jX_2 & 0 & -1 \\ R_1 & R_2 & Z_3 & 0 \\ V_1(h) & V_2(h) & V_3(h) & -\cos kh \end{bmatrix} \begin{bmatrix} A_1 \\ A_2 \\ A_3 \\ C_1 \end{bmatrix} = \begin{bmatrix} V_0 \\ 0 \\ 0 \\ V_0 \sin kh \end{bmatrix} \quad (24.6.12)$$

The matrix elements can be determined by evaluating the defining approximations (24.6.11) at z -points at which the currents $I_i(z)$ take on their maximum values. For $I_1(z)$, the maximum occurs at $z_1 = 0$ if $h \leq \lambda/4$ and at $z_1 = h - \lambda/4$ if $\lambda/4 \leq h \leq 5\lambda/8$.

For $I_2(z)$ and $I_3(z)$, the maxima occur at $z = 0$. Thus, the defining equations for the matrix elements are:

$$\begin{aligned} V_{d1}(z_1) &= V_1(z_1) - V_1(h) = R_1 I_3(z_1) + jX_1 I_1(z_1) \\ V_{d2}(0) &= V_2(0) - V_2(h) = R_2 I_3(0) + jX_2 I_2(0) \\ V_{d3}(0) &= V_3(0) - V_3(h) = Z_3 I_3(0) \end{aligned} \tag{24.6.13}$$

The coefficients R_1, X_1, R_2, X_2 are obtained by extracting the real and imaginary parts of these expressions. The left-hand sides can be computed by direct numerical integration of the definitions (24.6.7). The expected range of applicability of the 3-term approximation is for antenna lengths $l \leq 1.25\lambda$ (see [4,94].) However, it works well even for longer lengths.

The MATLAB function `king` implements the design equations (24.6.12) and (24.6.13). It has usage:

```
A = king(L,a); % King's 3-term sinusoidal approximation
```

where L, a are the antenna length and its radius in units of λ and the output A is the column vector of the coefficients A_i of the (unprimed) representation (24.6.3) of the current.

The numerical integrations are done with a 32-point Gauss-Legendre quadrature integration routine implemented with the function `quadr`, which provides the appropriate weights and evaluation points for the integration.

Example 24.6.1: Fig. 24.6.1 compares the three-term approximation to the standard sinusoidal approximation, $I(z) = \sin(k(h - |z|))$, and to the exact numerical solution of Hallén's equation for the two cases of $l = \lambda$ and $l = 1.5\lambda$. The antenna radius was $a = 0.005\lambda$.

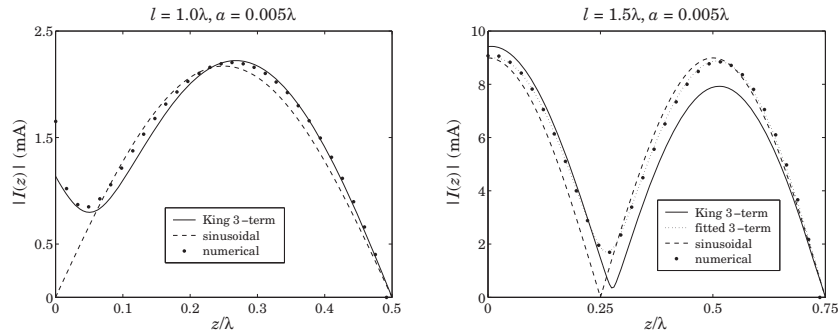


Fig. 24.6.1 Three-term approximation for $l = \lambda$ and $l = 1.5\lambda$.

In the full-wavelength case, the sinusoidal approximation has $I(0) = 0$, which would imply infinite antenna impedance. The three-term approximation gives a nonzero value for $I(0)$. The computed three-term coefficients are in the two cases:

$$\begin{bmatrix} A_1 \\ A_2 \\ A_3 \end{bmatrix} = 10^{-3} \begin{bmatrix} -2.6035j \\ 0.2737 + 0.2779j \\ 0.2666 + 0.2376j \end{bmatrix}, \quad \begin{bmatrix} A_1 \\ A_2 \\ A_3 \end{bmatrix} = 10^{-3} \begin{bmatrix} -2.1403j \\ 7.7886 - 3.6840j \\ 0.8688 + 2.4546j \end{bmatrix}$$

We used the unprimed representation for both cases (the primed one coincides with the unprimed one for the case $l = \lambda$ because $\cos kh = -1$ and the transformation matrix (24.6.5) becomes the identity matrix.) The graphs were generated by the following example code (for the $l = 1.5\lambda$ case):

```
L = 1.5; h = L/2; a = 0.005; % length and radius
k = 2*pi; % wavenumber in units of lambda = 1

M = 30; % number of cells is 2M + 1
[In,zn] = hdelta(L,a,M,'e'); % numerical solution of Hallen equation with exact kernel
In = In(M+1:end); % keep only upper half of the values
zn = zn(M+1:end);

A = king(L,a); % King's three-term approximation
z = 0:h/150:h; % evaluation points on upper half
Ik = abs(kingeval(L,A,z)); % evaluate King's three-term current

B = kingfit(L,In,zn,1); % fit one-term sinusoidal current
I1 = abs(kingeval(L,B,z)); % evaluate one-term sinusoidal current

C = kingfit(L,In,zn,3); % fit three-term current to the numerical values
I3 = abs(kingeval(L,C,z)); % evaluate fitted three-term current

plot(z,Ik,'-', z,I3,':', z,I1,'--', zn,abs(In), '.');
```

The currents $I_1(z)$ and $I_3(z)$ represent the one-term and three-term fits to the numerical samples I_n at the points z_n , as described below. □

As is evident from the above example, King's three-term approximation does not work particularly well for larger antenna lengths (about $l > 1.25\lambda$). This can be attributed to the crude approximation of computing the coefficients A_i by matching the defining currents only at one point along the antenna (at the current maxima).

It turns out, however, that the three-term approximation is very accurate if fitted to the "exact" current as computed by solving Hallén's equation numerically, with a range of applicability of up to about $l = 2\lambda$. With a 4-term fit, the range increases to $l = 3\lambda$.

Typically, numerical methods generate a set of N current values I_n at N points z_n , $n = 1, 2, \dots, N$, along the antenna. These values can be fitted to a three-term expression of the form of Eq. (24.6.3) using the least-squares criterion:

$$J = \sum_{n=1}^N |I_s(z_n) - I_n|^2 = \min, \quad \text{where } I_s(z) = \sum_{i=1}^3 A_i I_i(z) \tag{24.6.14}$$

where J is minimized with respect to the three coefficients A_1, A_2, A_3 . This is equivalent to finding the least-squares solution of the overdetermined $N \times 3$ linear system of equations (assuming $N > 3$):

$$\begin{bmatrix} I_1(z_1) & I_2(z_1) & I_3(z_1) \\ \vdots & \vdots & \vdots \\ I_1(z_n) & I_2(z_n) & I_3(z_n) \\ \vdots & \vdots & \vdots \\ I_1(z_N) & I_2(z_N) & I_3(z_N) \end{bmatrix} \begin{bmatrix} A_1 \\ A_2 \\ A_3 \end{bmatrix} = \begin{bmatrix} I_1 \\ \vdots \\ I_n \\ \vdots \\ I_N \end{bmatrix} \tag{24.6.15}$$

Writing this system in the compact matrix form $SA = I$, its MATLAB solution is obtained by the backslash operation: $A = S \setminus I$. More generally, one may perform the fit to $p = 1, 2, 3, 4$ sinusoidal terms, that is,

$$I_s(z) = \sum_{i=1}^p A_i I_i(z) \tag{24.6.16}$$

For $p = 1, 2, 3$, the basis currents $I_i(z)$ are as in Eq. (24.6.4). For $p = 1$, the basis is always defined as $I_1(z) = \sin(kh - k|z|)$. For $p = 4$, the first two basis currents, $I_1(z), I_2(z)$, are as in (24.6.4), and the last two are:

$$\begin{aligned} I_3(z) &= \cos(kz/4) - \cos(kh/4) \\ I_4(z) &= \cos(3kz/4) - \cos(3kh/4) \end{aligned} \tag{24.6.17}$$

The MATLAB function `kingfit` solves the system of equations (24.6.15), or its more general version, and returns the coefficients A_i . It has the following usage, where p is the desired number of terms:

```
A = kingfit(L, In, zn, p); % p-term fit to sinusoidal currents
```

The function `kingeval` evaluates the p -term approximation (24.6.16) at a given number of z -points:

```
I = kingeval(L, A, z); % evaluate p-term expression I(z) at the points z
```

where the number of terms p is determined from the number of coefficients A_i . The right graph of Fig. 24.6.1 compares King's and the least-squares three-term approximations.

The four-term approximation is justified as follows. The three-term case was based on the approximation $\sin kR/kR \simeq \cos(kR/2)$. To improve it, we consider the identity:

$$\frac{\sin kR}{kR} = \frac{\sin(kR/2)}{kR/2} \cos(kR/2) = \frac{\sin(kR/4)}{kR/4} \cos(kR/4) \cos(kR/2)$$

The three-term case is obtained by replacing $\sin(kR/2)/(kR/2) \simeq 1$, which is approximately valid for $R \leq \lambda/2$. A better approximation is obtained from the second identity by setting $\sin(kR/4)/(kR/4) \simeq 1$. This results in the approximation:

$$\frac{\sin kR}{kR} \simeq \cos(kR/4) \cos(kR/2) = \frac{1}{2} [\cos(kR/4) + \cos(3kR/4)] \tag{24.6.18}$$

which is well satisfied up to $R \leq 3\lambda/2$. Using the same arguments that led to Eq. (24.6.2), we now obtain the approximation:

$$\frac{j\eta}{2\pi} \int_{-h}^h G_{\text{app}}(z - z') I(z') dz' \simeq R \cos\left(\frac{kz}{4}\right) + R' \cos\left(\frac{3kz}{4}\right) + jXI(z) \tag{24.6.19}$$

where R, R', X are appropriate constants. Thus, Hallén's equation (24.3.12) can be approximated as:

$$R \cos\left(\frac{kz}{4}\right) + R' \cos\left(\frac{3kz}{4}\right) + jXI(z) = V(z) = C_1 \cos kz + V_0 \sin k|z|$$

which implies that $I(z)$ can be written as the sum of four sinusoidal currents, $I_1(z), I_2(z)$, given by Eq. (24.6.3), and $I_3(z), I_4(z)$, given by (24.6.17).

Fig. 24.6.2 compares the three-term and four-term fits for the two antenna lengths $l = \lambda$ and $l = 3\lambda$. For the $l = \lambda$ case, the two fits are virtually indistinguishable. The antenna radius was $a = 0.005\lambda$ and the "exact" numerical solution was computed using the exact kernel with $2M + 1 = 101$ segments. The graphs can be generated by the following example code:

```
L=3; a=0.005; M=50;
[IE, z] = hdel(L, a, M, 'e'); % solve Hallén equation with exact kernel and delta-gap input
A = kingfit(L, IE, z, 3); I3 = kingeval(L, A, z);
B = kingfit(L, IE, z, 4); I4 = kingeval(L, B, z);
plot(z, real(IE), '.', z, real(I4), '--', z, real(I3), '--');
```

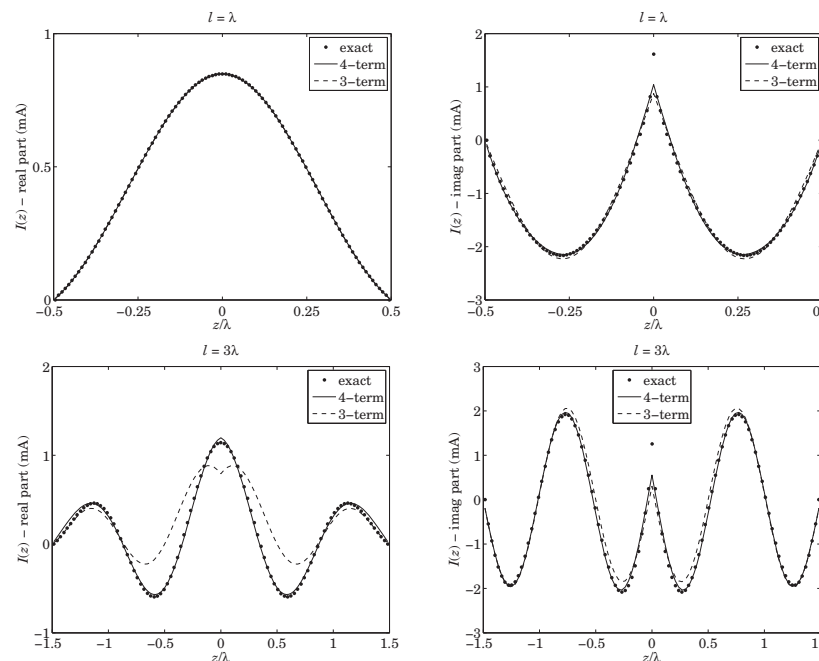


Fig. 24.6.2 Three- and four-term approximations for $l = \lambda$ and $l = 3\lambda$.

We will look at further examples later on. The main advantage of such fits is that they provide simple analytical expressions for the current, which can be used in turn to compute the radiation pattern. We saw in Eq. (17.1.7) that the radiation intensity of a

linear antenna is given by

$$U(\theta) = \frac{\eta k^2}{32\pi^2} |F_z(\theta)|^2 \sin^2 \theta$$

where $F_z(\theta)$ is the z-component of the radiation vector:

$$F_z(\theta) = \int_{-h}^h I(z) e^{jkz \cos \theta} dz$$

For the p -term current given by Eq. (24.6.16), we have:

$$F_z(\theta) = \sum_{i=1}^p A_i \int_{-h}^h I_i(z) e^{jkz \cos \theta} dz = \sum_{i=1}^p A_i F_i(\theta) \tag{24.6.20}$$

The individual radiation vectors $F_i(\theta)$ are given by closed-form expressions as follows. For $I_1(z)$ and $I'_1(z)$, we have:

$$\begin{aligned} F_1(\theta) &= \int_{-h}^h (\sin k|z| - \sin kh) e^{jkz \cos \theta} dz = \\ &= \frac{1}{k} \frac{(1 - \cos(kh \cos \theta) \cos kh) \cos \theta - \sin(kh \cos \theta) \sin kh}{\cos \theta \sin^2 \theta} \tag{24.6.21} \\ F'_1(\theta) &= \int_{-h}^h \sin(kh - k|z|) e^{jkz \cos \theta} dz = \frac{2}{k} \frac{\cos(kh \cos \theta) - \cos kh}{\sin^2 \theta} \end{aligned}$$

The rest of the radiation vectors are obtained from the following integral, with the parameter values $\alpha = 1, 1/2, 1/4, 3/4$:

$$\begin{aligned} &\int_{-h}^h [\cos(k\alpha z) - \cos(k\alpha h)] e^{jkz \cos \theta} dz = \\ &= \frac{\alpha}{k} \frac{(\alpha + \cos \theta) \sin(kh(\alpha - \cos \theta)) - (\alpha - \cos \theta) \sin(kh(\alpha + \cos \theta))}{\cos \theta (\alpha^2 - \cos^2 \theta)} \tag{24.6.22} \end{aligned}$$

24.7 Evaluation of the Exact Kernel

Numerical methods for Hallén's and Pocklington's equations require the numerical evaluation (and integration) of the exact or approximate kernel. A sample of such numerical methods is given in Refs. [1725-1788].

The evaluation of the approximate kernel is straightforward. The exact kernel requires a more careful treatment because of its singularity at $z = 0$. Here, we follow [1781] and express the exact kernel in terms of elliptic functions and discuss its numerical evaluation. The exact kernel was defined in Eq. (24.1.2):

$$G(z, \rho) = \frac{1}{2\pi} \int_0^{2\pi} \frac{e^{-jkR}}{R} d\phi', \quad R = \sqrt{z^2 + \rho^2 + a^2 - 2\rho a \cos \phi'} \tag{24.7.1}$$

The distance R may be written in the alternative forms:

$$\begin{aligned} R &= \sqrt{z^2 + (\rho + a)^2 - 2\rho a (1 + \cos \phi')} \\ &= \sqrt{z^2 + (\rho + a)^2 - 4\rho a \cos^2(\phi'/2)} \\ &= \sqrt{z^2 + (\rho + a)^2 - 4\rho a \sin^2 \theta} \\ &= R_{\max} \sqrt{1 - \kappa^2 \sin^2 \theta} \end{aligned} \tag{24.7.2}$$

where we defined:

$$R_{\max} = \sqrt{z^2 + (\rho + a)^2}, \quad \kappa = \frac{2\sqrt{a\rho}}{R_{\max}} = \frac{2\sqrt{a\rho}}{\sqrt{z^2 + (\rho + a)^2}} \tag{24.7.3}$$

and made the change of variables $\phi' = \pi + 2\theta$. Under this change, the integration range $[0, 2\pi]$ in ϕ' maps onto $[-\pi/2, \pi/2]$ in θ , and because R is even in θ , that range can be further reduced to $[0, \pi/2]$, resulting into the expression for the kernel:

$$G(z, \rho) = \frac{2}{\pi} \int_0^{\pi/2} \frac{e^{-jkR}}{R} d\theta = \frac{2}{\pi R_{\max}} \int_0^{\pi/2} \frac{e^{-jkR_{\max} \sqrt{1 - \kappa^2 \sin^2 \theta}}}{\sqrt{1 - \kappa^2 \sin^2 \theta}} d\theta \tag{24.7.4}$$

where R_{\max} represents the maximum value of R as θ varies. The approximate kernel corresponds to the limit $a = 0$ or $\kappa = 0$. The connection to elliptic functions comes about as follows [1790-1794]. The change of variables,

$$u = \int_0^\theta \frac{d\alpha}{\sqrt{1 - \kappa^2 \sin^2 \alpha}} \Rightarrow du = \frac{d\theta}{\sqrt{1 - \kappa^2 \sin^2 \theta}} \tag{24.7.5}$$

defines θ indirectly as a function of u . The Jacobian elliptic functions $\text{sn}(u, \kappa)$ and $\text{dn}(u, \kappa)$ are then defined by

$$\begin{aligned} \text{sn}(u, \kappa) &= \sin \theta \\ \text{dn}(u, \kappa) &= \sqrt{1 - \kappa^2 \text{sn}^2(u, \kappa)} = \sqrt{1 - \kappa^2 \sin^2 \theta} \end{aligned} \tag{24.7.6}$$

where κ is referred to as the elliptic *modulus*. The complete elliptic integrals of the first and second kinds are given by:

$$K(\kappa) = \int_0^{\pi/2} \frac{d\theta}{\sqrt{1 - \kappa^2 \sin^2 \theta}}, \quad E(\kappa) = \int_0^{\pi/2} \sqrt{1 - \kappa^2 \sin^2 \theta} d\theta \tag{24.7.7}$$

Thus, when $\theta = \pi/2$, then $u = K(\kappa)$. With these definitions, Eq. (24.7.4) can be written as:

$$G(z, \rho) = \frac{2}{\pi R_{\max}} \int_0^{K(\kappa)} e^{-jkR_{\max} \text{dn}(u, \kappa)} du \tag{24.7.8}$$

Changing variables from u to $uK(\kappa)$, we may write:

$$G(z, \rho) = \frac{2K(\kappa)}{\pi R_{\max}} \int_0^1 e^{-jkR_{\max} \text{dn}(uK, \kappa)} du \tag{24.7.9}$$

For points on the surface of the antenna wire ($\rho = a$), the kernel and the quantities R_{\max} and κ simplify into:

$$G(z) = \frac{2}{\pi} \int_0^{\pi/2} \frac{e^{-jkR}}{R} d\theta = \frac{2K(\kappa)}{\pi R_{\max}} \int_0^1 e^{-jkR_{\max} \operatorname{dn}(uK, \kappa)} du \quad (\text{exact kernel}) \quad (24.7.10)$$

with $R = \sqrt{z^2 + 4a^2 - 4a^2 \sin^2 \theta} = R_{\max} \sqrt{1 - \kappa^2 \sin^2 \theta}$ and

$$R_{\max} = \sqrt{z^2 + 4a^2}, \quad \kappa = \frac{2a}{R_{\max}} = \frac{2a}{\sqrt{z^2 + 4a^2}} \quad (24.7.11)$$

As u varies over the interval $0 \leq u \leq 1$, the quantity $\operatorname{dn}(uK, \kappa)$ stays bounded, varying over the range:

$$\kappa' \leq \operatorname{dn}(uK, \kappa) \leq 1 \quad (24.7.12)$$

where we introduced the *complementary* modulus:

$$\kappa' = \sqrt{1 - \kappa^2} = \frac{|z|}{\sqrt{z^2 + 4a^2}} = \frac{|z|}{R_{\max}} \quad (24.7.13)$$

Therefore, the integral in Eq. (24.7.10) remains bounded and less than one in magnitude for all values of z . On the other hand, the factor $K(\kappa)$ incorporates the logarithmic singularity at $z = 0$. Indeed, as $z \rightarrow 0$, the moduli κ and κ' tend to 1 and 0, respectively, and $K(\kappa)$ behaves as $\ln(4/\kappa')$ [1793]:

$$K(\kappa) \simeq \ln\left(\frac{4}{\kappa'}\right) \simeq \ln\left(\frac{4R_{\max}}{|z|}\right) \simeq \ln\left(\frac{8a}{|z|}\right), \quad \text{as } z \rightarrow 0 \quad (24.7.14)$$

where we replaced $R_{\max} \simeq 2a$ as $z \rightarrow 0$. Thus, the kernel behaves like

$$G(z) \simeq \frac{1}{\pi a} \ln\left(\frac{8a}{|z|}\right), \quad \text{as } z \rightarrow 0 \quad (24.7.15)$$

The MATLAB function `kernel` implements Eq. (24.7.10) to compute $G(z)$ at any vector of z points. For smaller values of z , it uses the asymptotic form (24.7.15). It has usage:

```
G = kernel(z,a,'e'); % exact kernel
G = kernel(z,a,'a'); % approximate kernel
```

It employs the following set of MATLAB functions for the evaluation of the complete elliptic integrals and the function $\operatorname{dn}(uK, \kappa)$:

```
K = ellipK(k); % elliptic integral K(k) at a vector of k's
E = ellipE(k); % elliptic integral E(k) at a vector of k's
v = landenv(k); % Landen transformations of a vector of k's
w = snv(u,k); % sn(uK, kappa) function at a vector of u's and a vector of k's
w = dnv(u,k); % dn(uK, kappa) function at a vector of u's and a vector of k's
```

These are based on a set of similar functions developed for the implementation of elliptic filters [1795-1797] that were modified here to handle a vector of moduli κ arising from a vector of z points. Using these functions, the integral in Eq. (24.7.10) is implemented with a 32-point Gauss-Legendre integration over the interval $0 \leq u \leq 1$. Let $w_i, u_i, i = 1, 2, \dots, 32$, denote the weights and evaluation points obtained by calling the quadrature function `quadr`:

```
[w,u] = quadr(0,1,32); % 32-point Gauss-Legendre integration over the interval [0,1]
```

Then, Eq. (24.7.10) can be evaluated by

$$G(z) = \frac{2K(\kappa)}{\pi R_{\max}} \sum_{i=1}^{32} w_i e^{-jkR_{\max} \operatorname{dn}(u_i K, \kappa)} \quad (24.7.16)$$

The function `kernel` has an additional input parameter, `method`,

```
G = kernel(z,a,'e',method); % exact kernel
```

that allows one to select faster but somewhat less accurate methods of computing the kernel. The method of Eq. (24.7.16) is selected with `method = 3`. The integral in (24.7.10) can be expanded approximately as follows [1781]:

$$\begin{aligned} J(\kappa) &= K \int_0^1 e^{-jkR_{\max} \operatorname{dn}(uK, \kappa)} du = \int_0^K e^{-jkR_{\max} \operatorname{dn}(u, \kappa)} du \\ &= e^{-jkR_{\max}} \int_0^K e^{-jkR_{\max} (\operatorname{dn}(u, \kappa) - 1)} du \\ &\simeq e^{-jkR_{\max}} \int_0^K \left[1 - jkR_{\max} (\operatorname{dn}(u, \kappa) - 1) + \frac{(-jkR_{\max})^2}{2} (\operatorname{dn}(u, \kappa) - 1)^2 \right] du \end{aligned}$$

Using the definitions (24.7.5)–(24.7.7), we find:

$$\int_0^K (\operatorname{dn}(u, \kappa) - 1) du = \frac{\pi}{2} - K, \quad \int_0^K (\operatorname{dn}(u, \kappa) - 1)^2 du = K + E - \pi$$

Thus, $J(\kappa)$ can be written approximately as

$$J(\kappa) = \int_0^K e^{-jkR_{\max} \operatorname{dn}(u, \kappa)} du \simeq e^{-jkR_{\max}} \left[K + jkR_{\max} \left(K - \frac{\pi}{2} \right) + \frac{(jkR_{\max})^2}{2} (K + E - \pi) \right]$$

This leads to the following approximations for the kernel $G(z)$. If only the linear term in (jkR_{\max}) is kept, then

$$G(z) = \frac{2e^{-jkR_{\max}}}{\pi R_{\max}} \left[K + jkR_{\max} \left(K - \frac{\pi}{2} \right) \right] \quad (24.7.17)$$

and, if both the linear and the quadratic terms are kept,

$$G(z) = \frac{2e^{-jkR_{\max}}}{\pi R_{\max}} \left[K + jkR_{\max} \left(K - \frac{\pi}{2} \right) + \frac{(jkR_{\max})^2}{2} (K + E - \pi) \right] \quad (24.7.18)$$

Eqs. (24.7.17) and (24.7.18) are selected with the `method = 1, 2`, respectively, and provide faster alternatives to the slower but more accurate method of Eq. (24.7.16).

Because $\kappa^2 = 1 - \kappa'^2$, floating point accuracy limits the values of κ'^2 to be greater than about the machine epsilon, that is, $\kappa' > \sqrt{\epsilon}$, which for MATLAB gives $\epsilon = 2.22 \times 10^{-16}$ and $\kappa' > \sqrt{\epsilon} = 1.49 \times 10^{-8}$. Since for small z we have $\kappa' = z/2a$, this limitation translates to a minimum value of z below which the elliptic function calculations cannot be used and one must use the asymptotic form (24.7.15):

$$\frac{z_{\min}}{2a} = \kappa' = \sqrt{\epsilon} \Rightarrow z_{\min} = (2.98 \times 10^{-8}) a \quad (24.7.19)$$

An alternative computation method, which will also help refine the asymptotic form (24.7.15), is based on a straightforward series expansion of the integral in (24.7.10):

$$J(\kappa) = K \int_0^1 e^{-jkR_{\max} \operatorname{dn}(u, \kappa)} du = \int_0^K e^{-jkR_{\max} \operatorname{dn}(u, \kappa)} du$$

$$= \sum_{m=0}^{\infty} \frac{(-jkR_{\max})^m}{m!} \int_0^K \operatorname{dn}^m(u, \kappa) du$$

Defining the integrals,

$$J_m(\kappa) = \int_0^K \operatorname{dn}^m(u, \kappa) du = \int_0^{\pi/2} \left(\sqrt{1 - \kappa^2 \sin^2 \theta} \right)^{m-1} d\theta, \quad m \geq 0 \quad (24.7.20)$$

we have:

$$J(\kappa) = \sum_{m=0}^{\infty} \frac{(-jkR_{\max})^m}{m!} J_m(\kappa) \quad (24.7.21)$$

The first few of these are:

$$J_0(\kappa) = K(\kappa)$$

$$J_1(\kappa) = \frac{\pi}{2}$$

$$J_2(\kappa) = E(\kappa) \quad (24.7.22)$$

$$J_3(\kappa) = \frac{\pi}{4} (1 + \kappa'^2)$$

$$J_4(\kappa) = \frac{1}{3} [2(1 + \kappa'^2)E(\kappa) - \kappa'^2 K(\kappa)]$$

where $\kappa'^2 = 1 - \kappa^2$. The rest can be computed from the following recursion [1793]:

$$J_{m+1}(\kappa) = \frac{(m-1)(1 + \kappa'^2)J_{m-1}(\kappa) - (m-2)\kappa'^2 J_{m-3}(\kappa)}{m}, \quad m \geq 4 \quad (24.7.23)$$

Separating the $m = 0$ term from the rest, the kernel can be written in the form:

$$G(z) = \frac{2}{\pi R_{\max}} (K(\kappa) + C(\kappa)), \quad C(\kappa) = \sum_{m=1}^{\infty} \frac{(-jkR_{\max})^m}{m!} J_m(\kappa) \quad (24.7.24)$$

In the limit $\kappa \rightarrow 1$, the quantities $J_m(\kappa)$ have a finite limit, with the exception of $J_0(\kappa)$, which diverges as $J_0(\kappa) = K(\kappa) = \ln(4/\kappa')$. For example, the term $\kappa'^2 K(\kappa)$ in $J_4(\kappa)$ converges to zero:

$$\lim_{\kappa \rightarrow 1} \kappa'^2 K(\kappa) = \lim_{\kappa' \rightarrow 0} \kappa'^2 \ln\left(\frac{4}{\kappa'}\right) = 0$$

In this limit, the integrals in (24.7.20) can be done in closed form and expressed in terms of the gamma function [1790]:

$$J_m(1) = \int_0^{\pi/2} (\cos \theta)^{m-1} d\theta = \frac{\sqrt{\pi}}{2} \frac{\Gamma\left(\frac{m}{2}\right)}{\Gamma\left(\frac{m+1}{2}\right)}, \quad m \geq 1 \quad (24.7.25)$$

Therefore, the term $C(\kappa)$ in (24.7.24) also has a finite limit given by:

$$C(1) = \sum_{m=1}^{\infty} \frac{(-2jka)^m}{m!} J_m(1) \quad (24.7.26)$$

where we replaced $R_{\max} = 2a$. Then, the asymptotic form (24.7.15) of the kernel may be modified by adding the constant $C(1)$:

$$G(z) = \frac{1}{\pi a} \left[\ln\left(\frac{8a}{|z|}\right) + C(1) \right], \quad \text{as } z \rightarrow 0 \quad (24.7.27)$$

In the function kernel, we use this approximation for $|z| < z_{\min}$, where the series for $C(1)$ converges very fast requiring about 4-5 terms for typical values of the radius, such as $0.001\lambda \leq a \leq 0.01\lambda$.

For $|z| \geq z_{\min}$, one may use the series expansion (24.7.24). The smaller the z , the smaller the number of terms required for convergence of the sum. For example, for the case $a = 0.005\lambda$ and for some typical values of z , the number of terms were:

z/λ	3	2	1	0.5	0.05	0.005	0.0005
M	76	58	38	22	10	7	7

The method (24.7.24) is selected by the value `method = 4` in the function `kernel`. We have included all four methods described by Eqs. (24.7.16)–(24.7.18), and (24.7.24) as options in `kernel`. The default method is that of Eq. (24.7.18) selected with `method = 2`.

24.8 Method of Moments

The method of moments (MoM) refers to a family of numerical methods for solving integral equations [1734–1740]. We summarize the method in the context of solving Hallén's equations for a delta-gap input, and later on, we apply it to the cases of arbitrary incident fields and Pocklington's equation. For an antenna of length l , half-length $h = l/2$, and radius a , Hallén's equation reads:

$$\frac{j\eta}{2\pi} \int_{-h}^h G(z - z') I(z') dz' = V(z) = C_1 \cos kz + V_0 \sin k|z| \quad (24.8.1)$$

where $G(z - z')$ is the exact or the approximate kernel. The antenna is divided into $N = 2M + 1$ segments of width $\Delta = l/N = 2h/(2M + 1)$, as shown in Fig. 24.8.1, with centers at the positions:

$$z_m = m\Delta, \quad -M \leq m \leq M \quad (24.8.2)$$

and the current is expanded into a sum of basis functions:

$$I(z') = \sum_{m=-M}^M I_m B(z' - z_m) \quad (24.8.3)$$

where $B(z' - z_m)$ are localized functions centered on the m th segment. For example, in the case of pulse basis functions shown in Fig. 24.8.1, we have:

$$B(z' - z_m) = \begin{cases} 1, & \text{if } |z' - z_m| \leq \frac{1}{2}\Delta \\ 0, & \text{otherwise} \end{cases} \quad (24.8.4)$$

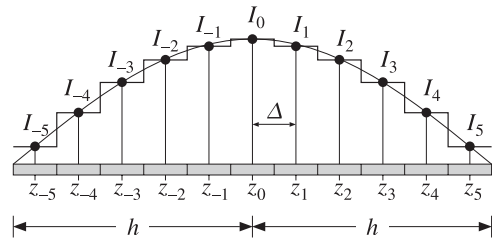


Fig. 24.8.1 Pulse-function segments along an antenna, with $N = 11, M = 5$.

Other basis functions are possible such as triangular, sinusoidal, or even plain delta-functions, and we will consider them in succeeding sections. Because of the localized nature of the basis, the expansion (24.8.3) is referred to as a *sub-domain* expansion. Alternatively, *entire-domain* basis functions can be used that are defined over the entire length l of the antenna. Substitution of $I(z')$ into the Hallén equation gives:

$$\frac{j\eta}{2\pi} \sum_{m=-M}^M I_m \int_{-h}^h G(z-z') B(z'-z_m) dz' = V(z) \tag{24.8.5}$$

The localized nature of $B(z'-z_m)$ restricts this integral to be over the m th segment. Next, a *local weighted average* is formed about each point $z_n = n\Delta$ by using another local weighting (or testing) function $W(z-z_n)$, which is centered on z_n :

$$\frac{j\eta}{2\pi} \sum_{m=-M}^M I_m \int_{-h}^h \int_{-h}^h W(z-z_n) G(z-z') B(z'-z_m) dz dz' = \int_{-h}^h W(z-z_n) V(z) dz$$

This may be written in the $N \times N$ matrix form:

$$\sum_{m=-M}^M Z_{nm} I_m = v_n, \quad -M \leq n \leq M \tag{24.8.6}$$

where we defined

$$Z_{nm} = \frac{j\eta}{2\pi} \int_{-h}^h \int_{-h}^h W(z-z_n) G(z-z') B(z'-z_m) dz dz' \tag{24.8.7}$$

$$v_n = \int_{-h}^h W(z-z_n) V(z) dz$$

Two popular choices for the weighting function are the Galerkin and the point-matching or collocation choices. In the Galerkin method the weighting function is taken to be the same as the basis function, and in the point-matching case, it is a delta function:

$$\begin{aligned} W(z-z_n) &= \delta(z-z_n) && \text{(point-matching)} \\ W(z-z_n) &= B(z-z_n) && \text{(Galerkin)} \end{aligned} \tag{24.8.8}$$

Thus, in the *point-matching method*, Eqs. (24.8.7) reduce to:

$$Z_{nm} = \frac{j\eta}{2\pi} \int_{-h}^h G(z_n-z') B(z'-z_m) dz' \tag{24.8.9}$$

$$v_n = V(z_n) = C_1 \cos kz_n + V_0 \sin k|z_n|$$

Similarly, in the *Galerkin method*, we have:

$$Z_{nm} = \frac{j\eta}{2\pi} \int_{-h}^h \int_{-h}^h B(z-z_n) G(z-z') B(z'-z_m) dz dz' \tag{24.8.10}$$

$$v_n = \int_{-h}^h B(z-z_n) V(z) dz$$

In succeeding sections, we will consider the following cases and discuss how to compute the quantities Z_{nm} and v_n :

- Delta-function basis with point matching
- Pulse-function basis with point matching
- Pulse-function basis with Galerkin weighting
- Triangular basis with point matching
- Sinusoidal spline basis (NEC basis) with point matching
- Method of moments for Hallén's equation with arbitrary incident field
- Method of moments for Pocklington's equation

We will also consider the following issues that have been discussed extensively in the literature regarding the existence of solutions of Hallén's equation (24.8.1) with delta-gap input [1765-1777]:

1. The approximate kernel is non-singular at $z = 0$. Yet, the numerical solution of Hallén's equation using the approximate kernel does not converge and becomes unusable for increasing number of segments N and/or for increasing radius a , whereas the solution based on the exact kernel does converge. However, for moderate values of N , one does get useful results from the approximate kernel.
2. In fact, the approximate-kernel Hallén equation for a delta-gap input does not, strictly speaking, have a solution, whereas the one with the exact kernel does.
3. The input impedance of the antenna, $Z_0 = V_0/I(0)$, for the delta-gap case does not converge to a constant value for the approximate kernel as N increases, but it does so for the exact kernel. Generally, numerical methods get the resistive part of Z_0 fairly accurately, but have a hard time for the reactive part.
4. The solution $I(z)$ for the exact kernel in the delta-gap case has a logarithmic singularity at $z = 0$ of the form:

$$I(z) \simeq -j \frac{4kaV_0}{\eta} \ln(k|z|), \quad z \simeq 0 \tag{24.8.11}$$

Therefore, one may wonder if the numerical solutions have any use. However, this logarithmic singularity is confined to a very narrow range around $z = 0$ and for all other values of z , the exact-kernel solution is accurate and useful.

- 5. King's empirical three-term approximation for the current is also very accurate (except in the immediate vicinity of the logarithmic singularity at $z = 0$), if fitted to the exact-kernel solution.

24.9 Delta-Function Basis

Here, we discuss numerical solutions of (24.8.1) using a delta-function basis with point matching. The basis functions are defined by:

$$B(z' - z_m) = \delta(z' - z_m) \Delta \tag{24.9.1}$$

Fig. 24.9.1 depicts the delta functions as narrow pulses of width δ . The factor Δ is needed to give $I(z')$ the right dimensions.

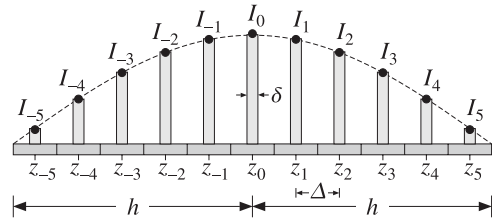


Fig. 24.9.1 Delta-function segments along an antenna, with $N = 11, M = 5$.

Inserting this basis into Eq. (24.8.9), we find

$$Z_{nm} = \frac{j\eta}{2\pi} G(z_n - z_m) \Delta, \quad -M \leq n, m \leq M \tag{24.9.2}$$

$$v_n = C_1 \cos kz_n + V_0 \sin k|z_n|, \quad -M \leq n \leq M$$

Because $z_n - z_m = (n - m)\Delta$, the diagonal entries Z_{nn} correspond to the evaluation of the kernel $G(z)$ at $z = 0$. For the approximate kernel, $G(0)$ is finite (corresponding to the small but finite radius $R = a$). But for the exact kernel, $G(0)$ is infinite because of its logarithmic singularity at $z = 0$. A reasonable way of modifying Z_{nn} is to replace the infinitely thin delta-function by a finite-width pulse:

$$B(z) = \delta(z) \Delta \rightarrow \frac{u(z + \delta/2) - u(z - \delta/2)}{\delta} \Delta$$

where $u(z)$ is the unit-step. Then, Eq. (24.9.3) gives in the case $n = m$:

$$Z_{nn} = \frac{j\eta}{2\pi} \int_{-h}^h G(z_n - z') B(z' - z_n) dz' = \frac{\Delta}{\delta} \frac{j\eta}{2\pi} \int_{-\delta/2}^{\delta/2} G(z) dz$$

where we used the even-ness of $G(z)$. The best choice for δ which yields results comparable to the other bases is the value $\delta = \Delta$, giving:

$$Z_{nm} = \frac{j\eta}{2\pi} \int_{-\Delta/2}^{\Delta/2} G(z) dz, \quad -M \leq n \leq M \tag{24.9.3}$$

We evaluate this integral numerically using Gauss-Legendre integration. However, one could also use quadrature rules [1755,1756] that are more appropriate for the logarithmic singularity of $G(z)$. The above method of regularizing the impedance matrix by local averaging about the singularity region is akin to alternative discretizations based on locally-corrected Nyström methods that replace the integral equation by a quadrature integration rule, such as Gauss-Legendre [1761-1764].

With the definitions (24.9.2) and (24.9.3), the matrix equation (24.8.6) may be written in the compact form:

$$Z\mathbf{I} = \mathbf{v} = C_1 \mathbf{c} + V_0 \mathbf{s} \tag{24.9.4}$$

where Z is the $N \times N$ matrix with matrix elements Z_{nm} and $\mathbf{I}, \mathbf{s}, \mathbf{c}$ are the column vectors with elements $I_n, c_n = \cos kz_n$, and $s_n = \sin k|z_n|$, for $n = -M, \dots, M$. The vector \mathbf{I} is symmetric about its middle, that is, $I_{-n} = I_n$, and similarly for \mathbf{c}, \mathbf{s} . Therefore, we have:

$$\mathbf{I} = \begin{bmatrix} I_M \\ \vdots \\ I_1 \\ I_0 \\ I_1 \\ \vdots \\ I_M \end{bmatrix}, \quad \mathbf{v} = \begin{bmatrix} v_M \\ \vdots \\ v_1 \\ v_0 \\ v_1 \\ \vdots \\ v_M \end{bmatrix}, \quad \mathbf{c} = \begin{bmatrix} c_M \\ \vdots \\ c_1 \\ c_0 \\ c_1 \\ \vdots \\ c_M \end{bmatrix}, \quad \mathbf{s} = \begin{bmatrix} s_M \\ \vdots \\ s_1 \\ s_0 \\ s_1 \\ \vdots \\ s_M \end{bmatrix} \tag{24.9.5}$$

The matrix Z is a symmetric Toeplitz matrix because the matrix element Z_{nm} depends only on the difference $|n - m|$. Taking advantage of the Toeplitz nature of Z and the symmetry of the vectors (24.9.5), the matrix system (24.9.4) can be replaced by one essentially half its size, thus, speeding up the solution. To see this, we partition the vector \mathbf{I} into its upper (negative- z), middle, and lower (positive- z) parts:

$$\mathbf{I} = \begin{bmatrix} \mathbf{I}_1^R \\ I_0 \\ \mathbf{I}_1 \end{bmatrix}, \quad \mathbf{I}_1 = \begin{bmatrix} I_1 \\ I_2 \\ \vdots \\ I_M \end{bmatrix}, \quad \mathbf{I}_1^R = \begin{bmatrix} I_M \\ \vdots \\ I_2 \\ I_1 \end{bmatrix}$$

The upper part \mathbf{I}_1^R is the reverse of the lower part \mathbf{I}_1 . The reversal operation can be expressed as a matrix operation:

$$\mathbf{I}_1^R = J\mathbf{I}_1, \quad J = \begin{bmatrix} 0 & \cdots & 0 & 1 \\ 0 & \cdots & 1 & 0 \\ \vdots & \ddots & \vdots & \vdots \\ 1 & \cdots & 0 & 0 \end{bmatrix}$$

where J is the $M \times M$ reversing matrix J , that is, the matrix with ones along its antidiagonal. Then, the impedance matrix Z and Eq. (24.9.4) can be partitioned in a compatible way as follows:

$$\begin{bmatrix} A^R & \mathbf{a}^R & B^R \\ \mathbf{a}^{TR} & a_0 & \mathbf{a}^T \\ B & \mathbf{a} & A \end{bmatrix} \begin{bmatrix} \mathbf{I}_1^R \\ I_0 \\ \mathbf{I}_1 \end{bmatrix} = \begin{bmatrix} \mathbf{v}_1^R \\ v_0 \\ \mathbf{v}_1 \end{bmatrix} \tag{24.9.6}$$

where we have separated the middle column and row of Z . Because Z satisfies the reversal invariance condition $Z(n, m) = Z(-n, -m)$, the upper-left block A^R will be the reverse of the lower-right block A , and the upper-right, the reverse of the lower-left. Moreover, because Z is symmetric, we have $A^R = A^T = A$ and $B^R = B^T$.

The reverse of a matrix is obtained by reversing its columns and then reversing its rows, an operation which is equivalent to multiplication by the reversing matrix J from left and right:

$$A^R = JAJ$$

Writing out the three sub-block equations of Eq. (24.9.6), we obtain:

$$\begin{aligned} A^R I_1^R + \mathbf{a}^R I_0 + B^R I_1 &= \mathbf{v}_1^R \\ \mathbf{a}^{TR} I_1^R + a_0 I_0 + \mathbf{a}^T I_1 &= \mathbf{v}_0 \\ B I_1^R + \mathbf{a} I_0 + A I_1 &= \mathbf{v}_1 \end{aligned}$$

But, the first is exactly the reverse of the last, and therefore redundant. Noting that $\mathbf{a}^{TR} I_1^R = \mathbf{a}^T I_1$ and $B I_1^R = B J I_1$, we obtain the reduced system:

$$\begin{aligned} a_0 I_0 + 2\mathbf{a}^T I_1 &= \mathbf{v}_0 \\ \mathbf{a} I_0 + (A + B J) I_1 &= \mathbf{v}_1 \end{aligned}$$

which can be written in the reduced block matrix form:

$$\begin{bmatrix} a_0 & 2\mathbf{a}^T \\ \mathbf{a} & A + B J \end{bmatrix} \begin{bmatrix} I_0 \\ I_1 \end{bmatrix} = \begin{bmatrix} \mathbf{v}_0 \\ \mathbf{v}_1 \end{bmatrix} \tag{24.9.7}$$

Thus, we can replace the $N \times N$ system (24.9.4) or (24.9.6) by the $(M + 1) \times (M + 1)$ system (24.9.7) acting only on half-vectors. We will write Eq. (24.9.7) in the following compact form:

$$\boxed{Z\mathbf{I} = \mathbf{v} = C_1 \mathbf{c} + V_0 \mathbf{s}} \tag{24.9.8}$$

where Z is constructed from Z according to (24.9.7) and the vectors are the half-vectors:

$$\mathbf{I} = \begin{bmatrix} I_0 \\ I_1 \\ \vdots \\ I_M \end{bmatrix}, \quad \mathbf{v} = \begin{bmatrix} v_0 \\ v_1 \\ \vdots \\ v_M \end{bmatrix}, \quad \mathbf{c} = \begin{bmatrix} c_0 \\ c_1 \\ \vdots \\ c_M \end{bmatrix}, \quad \mathbf{s} = \begin{bmatrix} s_0 \\ s_1 \\ \vdots \\ s_M \end{bmatrix} \tag{24.9.9}$$

Next, we impose the condition that $I_M = 0$ from which the constant C_1 can be determined. This condition can be written vectorially in the form $\mathbf{u}^T \mathbf{I} = 0$, where $\mathbf{u}^T = [0, \dots, 0, 1]$. Solving (24.9.8) for \mathbf{I} , we obtain:

$$\boxed{\mathbf{I} = C_1 Z^{-1} \mathbf{c} + V_0 Z^{-1} \mathbf{s}} \tag{24.9.10}$$

Multiplying both sides by \mathbf{u}^T , we obtain the condition:

$$\mathbf{u}^T \mathbf{I} = C_1 \mathbf{u}^T Z^{-1} \mathbf{c} + V_0 \mathbf{u}^T Z^{-1} \mathbf{s} = 0$$

which may be solved for C_1 :

$$\boxed{C_1 = -V_0 \frac{\mathbf{u}^T Z^{-1} \mathbf{s}}{\mathbf{u}^T Z^{-1} \mathbf{c}}} \tag{24.9.11}$$

The two equations (24.9.10) and (24.9.11) provide the complete solution of the discretized Hallén equation. The MATLAB function `hdel` implements the above solution procedure. It has usage:

```
[I,z,cnd] = hdel(L,a,M,ker,basis); % solve Hallén equation with delta-gap input
```

The string parameter inputs `ker` and `basis` take the possible values:

```
ker = 'e', 'a' % exact or approximate kernel
basis = 'p', 't', 'n', 'd' % pulse, triangular, NEC, or delta-function basis
```

where the choice `basis='d'` applies in this section. This function solves the half system (24.9.8), but returns the full N -dimensional symmetric vector \mathbf{I} of Eq. (24.9.5). The quantity \mathbf{z} is the N -dimensional vector of sampled z -points (24.8.2), and `cnd` is the condition number of the matrix Z that is being inverted. The quantities L, a are the antenna length and radius in units of λ , and M has the same meaning as above.

The matrix inversions required in (24.9.10) can be implemented efficiently by MATLAB's backslash operation `Z\[c,s]`. The function assumes $V_0 = 1$. Therefore, the input impedance of the antenna will be $Z_0 = V_0/I_0 = 1/I_0$, where I_0 is the middle of the output vector \mathbf{I} (i.e., the sample $I(M + 1)$ in MATLAB indexing.)

Internally, the function `hdel` calls the functions `hmat` and `hwrap` to construct the impedance matrices Z and Z :

```
[Z,B] = hmat(L,a,M,ker,basis); % construct the (2M+1) x (2M+1) Hallén impedance matrix
Zwrap = hwrap(Z); % wrap impedance matrix to size (M+1) x (M+1)
```

where B is a tridiagonal matrix that is applicable only in the NEC basis case, as explained in Sec. 24.12, and is equal to the identity matrix otherwise.

Fast Toeplitz solvers can also be used, based on the Levinson recursion and fast Cholesky factorizations [49]. However, we found that the built-in linear system solver of MATLAB is much faster for sizes of the order $M = 20$ – 200 .

Example 24.9.1: To clarify the structure of the impedance matrix Z and show how to wrap it efficiently into the half-size of (24.9.7), consider the case $N = 7$ or $M = 3$. Because Z is Toeplitz and symmetric, it can be built from the knowledge of its first column or first row. The first column is $Z_{n,-M} = Z_{n+M,0}$, for $-M \leq n \leq M$. Setting $m = n + M$, so that $m = 0, 1, \dots, 2M$, the first column (and first row) consists of the numbers:

$$a_m = Z_{m,0}, \quad m = 0, 1, \dots, 2M \tag{24.9.12}$$

Therefore, the full matrix Z will have the form:

$$Z = \begin{bmatrix} a_0 & a_1 & a_2 & a_3 & a_4 & a_5 & a_6 \\ a_1 & a_0 & a_1 & a_2 & a_3 & a_4 & a_5 \\ a_2 & a_1 & a_0 & a_1 & a_2 & a_3 & a_4 \\ a_3 & a_2 & a_1 & a_0 & a_1 & a_2 & a_3 \\ a_4 & a_3 & a_2 & a_1 & a_0 & a_1 & a_2 \\ a_5 & a_4 & a_3 & a_2 & a_1 & a_0 & a_1 \\ a_6 & a_5 & a_4 & a_3 & a_2 & a_1 & a_0 \end{bmatrix}$$

where we partitioned it as in Eq. (24.9.7), with submatrices:

$$A = \begin{bmatrix} a_0 & a_1 & a_2 \\ a_1 & a_0 & a_1 \\ a_2 & a_1 & a_0 \end{bmatrix}, \quad B = \begin{bmatrix} a_4 & a_3 & a_2 \\ a_5 & a_4 & a_3 \\ a_6 & a_5 & a_4 \end{bmatrix}, \quad \mathbf{a} = \begin{bmatrix} a_1 \\ a_2 \\ a_3 \end{bmatrix}$$

Therefore, the wrapped version of Z will be:

$$Z = \begin{bmatrix} a_0 & 2\mathbf{a}^T \\ \mathbf{a} & A + BJ \end{bmatrix} = \begin{bmatrix} a_0 & 2a_1 & 2a_2 & 2a_3 \\ a_1 & a_0 + a_2 & a_1 + a_3 & a_2 + a_4 \\ a_2 & a_1 + a_3 & a_0 + a_4 & a_1 + a_5 \\ a_3 & a_2 + a_4 & a_1 + a_5 & a_0 + a_6 \end{bmatrix} \quad (24.9.13)$$

This matrix can be constructed quickly as follows. Once the numbers $a_m, m = 0, 1, \dots, 2M$ are computed, take the first and last $M + 1$ numbers, that is, define the two row vectors:

$$\mathbf{f} = [a_0, a_1, a_2, a_3, a_4, a_5, a_6] \Rightarrow \mathbf{g} = [a_0, a_1, a_2, a_3], \quad \mathbf{h} = [a_3, a_4, a_5, a_6]$$

Then, form the Toeplitz matrix whose first column and first row are \mathbf{g} , and add it to the Hankel matrix whose first column is \mathbf{g} and last row is \mathbf{h} . This is accomplished easily by the built-in MATLAB functions `toeplitz` and `hankel`:

$$\text{toeplitz}(\mathbf{g}, \mathbf{g}) + \text{hankel}(\mathbf{g}, \mathbf{h}) = \begin{bmatrix} 2a_0 & 2a_1 & 2a_2 & 2a_3 \\ 2a_1 & a_0 + a_2 & a_1 + a_3 & a_2 + a_4 \\ 2a_2 & a_1 + a_3 & a_0 + a_4 & a_1 + a_5 \\ 2a_3 & a_2 + a_4 & a_1 + a_5 & a_0 + a_6 \end{bmatrix}$$

Then, replace the first column by half its value. These procedures are incorporated into the function `hwrap`. We note that the full matrix Z can also be constructed using the function `toeplitz` by:

$$Z = \text{toeplitz}(\mathbf{f}, \mathbf{f})$$

This is how Z is constructed by the function `hmat`. □

24.10 Pulse Basis

The delta function discretization scheme described in the previous section yields comparable results to the other bases. Here, we look at the pulse-function basis, which was defined by Eq. (24.8.4) and shown in Fig. 24.8.1. For the *point-matching case*, the matrix elements Z_{nm} are given by Eq. (24.8.9):

$$Z_{nm} = \frac{j\eta}{2\pi} \int_{-h}^h G(z_n - z') B(z' - z_m) dz' = \frac{j\eta}{2\pi} \int_{z_m - \Delta/2}^{z_m + \Delta/2} G(z_n - z') dz'$$

or, changing integration variable to $z = z' - z_m$,

$$Z_{nm} = \frac{j\eta}{2\pi} \int_{-\Delta/2}^{\Delta/2} G(z_n - z_m - z) dz, \quad -M \leq n, m \leq M \quad (24.10.1)$$

The integration range can be folded in half giving:

$$Z_{nm} = \frac{j\eta}{2\pi} \int_0^{\Delta/2} [G(z_n - z_m - z) + G(z_n - z_m + z)] dz \quad (24.10.2)$$

The function `hmat` with the option, `basis='p'`, may be used to evaluate Z_{nm} , for both the exact and the approximate kernels. A 32-point Gauss-Legendre quadrature integration rule is used to evaluate the integral in (24.10.2). The Hallén matrix equation is again given by (24.9.4):

$$Z\mathbf{I} = \mathbf{v} = C_1\mathbf{c} + V_0\mathbf{s} \quad (24.10.3)$$

and may be solved using the techniques of the previous sections. The function `hdel` solves (24.10.3) with the option, `basis='p'`.

For the *Galerkin case*, the matrix equation (24.10.3) has the same form but with some redefinitions of the quantities $Z, \mathbf{c}, \mathbf{s}$. The matrix elements Z_{nm} are given by (24.8.10):

$$\begin{aligned} Z_{nm} &= \frac{j\eta}{2\pi} \int_{-h}^h \int_{-h}^h B(z - z_n) G(z - z') B(z' - z_m) dz dz' = \\ &= \frac{j\eta}{2\pi} \int_{z_n - \Delta/2}^{z_n + \Delta/2} \int_{z_m - \Delta/2}^{z_m + \Delta/2} G(z - z') dz dz' \\ &= \frac{j\eta}{2\pi} \int_{-\Delta/2}^{\Delta/2} \int_{-\Delta/2}^{\Delta/2} G(z_n - z_m + x - x') dx dx' \end{aligned}$$

where we changed variables to $x = z - z_n$ and $x' = z' - z_m$. Defining a new integration variable $z = x - x'$, then one of the remaining integrations can be done giving:

$$Z_{nm} = \frac{j\eta}{2\pi} \int_{-\Delta}^{\Delta} (\Delta - |z|) G(z_n - z_m + z) dz, \quad -M \leq n, m \leq M \quad (24.10.4)$$

Similarly, the right-hand side vector \mathbf{v} of (24.10.3) has components:

$$\begin{aligned} v_n &= \int_{-h}^h B(z - z_n) V(z) dz = \int_{-\Delta/2}^{\Delta/2} V(z_n + x) dx \\ &= C_1 \int_{-\Delta/2}^{\Delta/2} \cos k(z_n + x) dx + V_0 \int_{-\Delta/2}^{\Delta/2} \sin k|z_n + x| dx \equiv C_1 c_n + V_0 s_n \end{aligned}$$

where the individual terms c_n, s_n can be calculated explicitly:

$$\begin{aligned} c_n &= \int_{-\Delta/2}^{\Delta/2} \cos k(z_n + x) dx = \frac{2}{k} \sin\left(\frac{k\Delta}{2}\right) \cos kz_n \\ s_n &= \int_{-\Delta/2}^{\Delta/2} \sin k|z_n + x| dx = \frac{4}{k} \sin^2\left(\frac{k\Delta}{4}\right) \delta(n) + \frac{2}{k} \sin\left(\frac{k\Delta}{2}\right) \sin k|z_n| \end{aligned} \quad (24.10.5)$$

where $\delta(n)$ is the Kronecker delta, and $z_n = n\Delta$, for $-M \leq n \leq M$. The Galerkin method yields very comparable results to the point matching case.

Some examples of the point-matching case with pulse-function basis were shown in Figs. 24.6.1 and 24.6.2. Some further examples are given below based on [1774,1775].

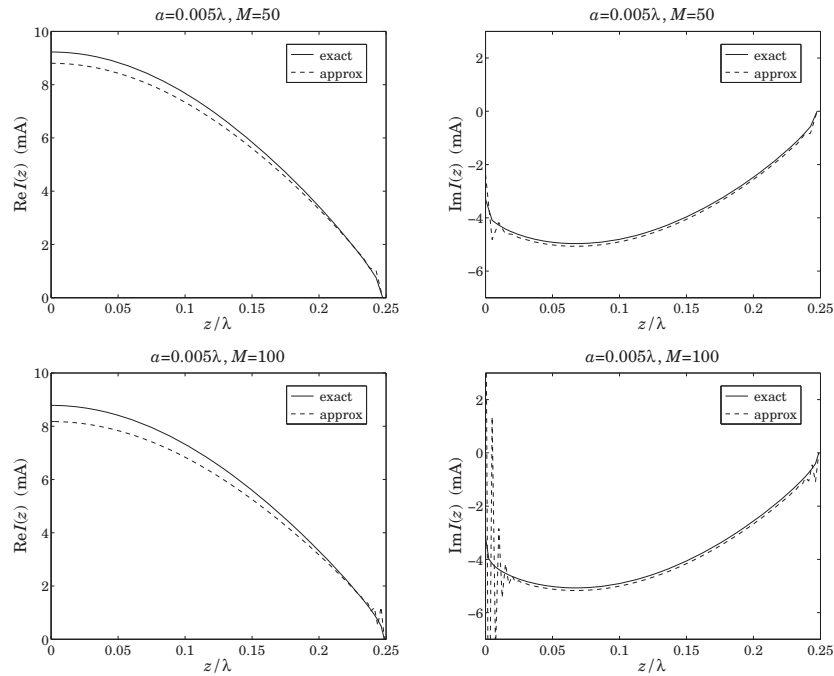


Fig. 24.10.1 Real and imaginary parts of $I(z)$ for half-wave dipole, $M = 50$ and $M = 100$.

Fig. 24.10.1 compares the solutions of (24.10.3) using the exact and the approximate kernels for a dipole of length $l = 0.5\lambda$ and radius $a = 0.005\lambda$.

The upper two graphs show the real and imaginary parts of the current samples I_n (joined here by straight lines) using $M = 50$, which corresponds to $N = 2M + 1 = 101$ segments. The lower two graphs show the case of $M = 100$. We note that for the approximate kernel, the solution oscillates wildly near the center and the end-points of the antenna—a behavior attributed to the non-existence of solutions of the Hallén equation Eq. (24.8.1) in this case. Fig. 24.10.2 depicts the case of a half-wave dipole with a larger radius $a = 0.008\lambda$ and $M = 100$, for which the oscillations get worse.

We have not superimposed King's three-term fit because it is virtually indistinguishable from the exact-kernel solution. The graphs, including the 3-term fit, may be generated by the following example MATLAB code:

```
L=0.5; a=0.005; M=100;
[Ie,z] = hdel $\tau$ (L,a,M,'e','p'); % solution of Hallén equation with exact kernel
Ia = hdel $\tau$ (L,a,M,'a','p'); % solution of Hallén equation with approximate kernel
A = kingfit(L,Ie,z,3); % three-term coefficients fitted to exact-kernel solution
I3 = kingeval(L,A,z); % evaluate 3-term current at the sample points z

figure; plot(z,real(Ie),'-', z,real(Ia),':', z,real(I3),'--');
figure; plot(z,imag(Ie),'-', z,imag(Ia),':', z,imag(I3),'--');
```

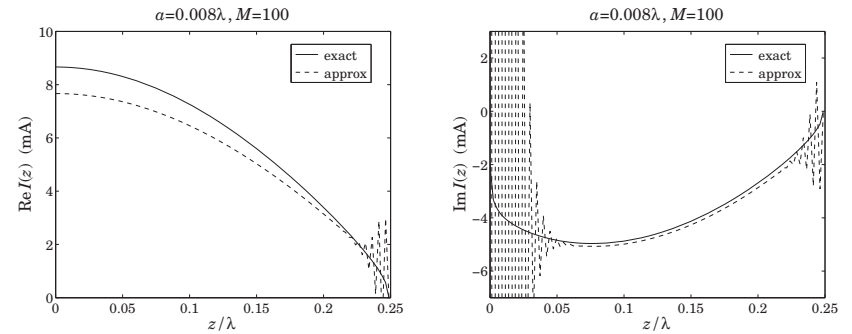


Fig. 24.10.2 Current on half-wave dipole of radius $a = 0.008\lambda$ and $M = 100$.

In Fig. 24.10.3, we compare how well the logarithmic behavior of Eq. (24.8.11) near $z = 0$ fits the computed current $I(z)$.

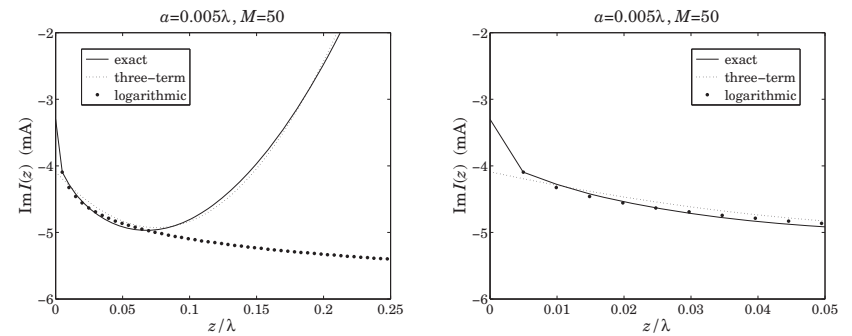


Fig. 24.10.3 Logarithmic behavior of the solution near $z = 0$.

To make the comparison, we adjust the asymptotic form (24.8.11) to match the computed value at the the closest z -point to zero, that is, at $z_1 = \Delta$. The adjusted asymptotic current is then,

$$I_{\log}(z) \approx -j \frac{4kaV_0}{\eta} \ln \left| \frac{z}{z_1} \right| + I(z_1), \quad z \approx 0 \quad (24.10.6)$$

so that it satisfies $I_{\log}(z_1) = I(z_1)$. For the case $a = 0.005\lambda$ and $M = 50$, Fig. 24.10.3 plots the imaginary part of the computed current $I(z)$ based on the exact kernel, together with the corresponding three-term fit, and the asymptotic current $I_{\log}(z)$.

The graph on the left is over the interval $0 \leq z \leq 0.25\lambda$, whereas the graph on the right shows only the narrow interval $0 \leq z \leq 0.05\lambda$, and both graphs use an expanded vertical scale compared to that of Fig. 24.10.1. The logarithmic behavior is evident. We note also that the three-term fit agrees very well with the computed current except in a narrow interval about $z = 0$.

Finally, we look at the stability of the numerical solutions based on the exact and approximate kernels as the number of segments M increases. Fig. 24.10.4 depicts the calculated input admittance $Y_0 = I_0/V_0$ as a function of the number of segments M .

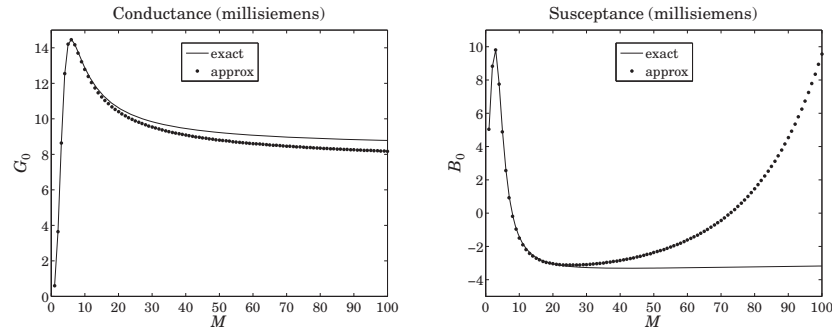


Fig. 24.10.4 Input admittance of half-wave dipole vs. number of segments M .

The conductance $G_0 = \text{Re}(Y_0)$ converges for both the exact and approximate kernel solutions. However, the susceptance $B_0 = \text{Im}(Y_0)$ diverges for the approximate kernel case, and converges for the exact kernel—the two agreeing well only for $M \leq 30$.

Fig. 24.10.5 depicts the dependence of the condition number of the Hallén impedance matrix Z on the number of segments M . We note the relative well-conditioning of the exact-kernel case. The above graphs may be computed with the following MATLAB code:

```
L=0.5; a=0.005;
for M=1:1:100,
    [I,z,cnd] = hdelat(L,a,M,'e','p'); Ye(M) = I(M+1); ce(M) = cnd;
    [I,z,cnd] = hdelat(L,a,M,'a','p'); Ya(M) = I(M+1); ca(M) = cnd;
end
M=1:1:100;
figure; plot(M,real(Ye),'-', M,real(Ya),'.');
figure; plot(M,imag(Ye),'-', M,imag(Ya),'.');
figure; semilogy(M,ce,'-', M,ca,'--');
```

For very small antenna radius, the exact and approximate kernels produce essentially the same current solutions. Fig. 24.10.6 shows the input impedance $Z_0 = R + jX = V_0/I_0$ versus the antenna length in the interval $0.3\lambda \leq l \leq 0.7\lambda$, and for the two radii $a = 0.0005\lambda$ and 0.00001λ .

The calculation was carried out using a pulse basis and the approximate kernel with $M = 100$ segments, but one could just as well have used the exact kernel or a triangular basis with very little difference in the results. The graphs are similar to those of Fig. 17.3.1 and show the resonant length at about 0.48λ - 0.49λ . The graphs were produced with the MATLAB code:

```
L = linspace(0.3,0.7,41);
a = [0.0005, 0.00001];
```

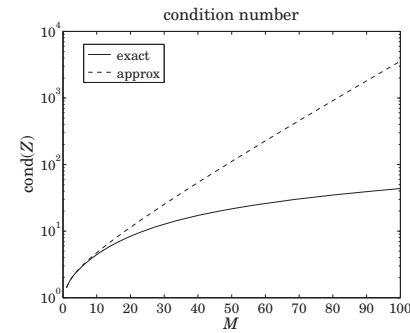


Fig. 24.10.5 Condition number of Hallén impedance matrix vs. number of segments M .

```
M = 100;
for i=1:length(L),
    for k=1:length(a),
        I = hdelat(L(i),a(k),M,'a','p'); Z(i,k) = 1/I(M+1);
    end
end
figure; plot(L, real(Z(:,1)), '- ', L, real(Z(:,2)), '--');
figure; plot(L, imag(Z(:,1)), '- ', L, imag(Z(:,2)), '--');
```

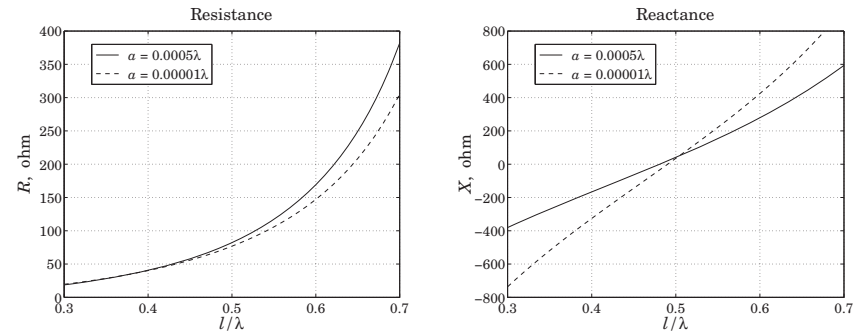


Fig. 24.10.6 Input impedance versus antenna length.

24.11 Triangular Basis

For the triangular basis, the current expansion (24.8.3), reads

$$I(z') = \sum_{m=-M}^M I_m B(z' - z_m) \tag{24.11.1}$$

where $B(z)$ is the triangular function:

$$B(z) = \begin{cases} 1 - \frac{|z|}{\Delta}, & \text{if } |z| \leq \Delta \\ 0, & \text{otherwise} \end{cases} \quad (24.11.2)$$

The triangular basis functions, depicted in Fig. 24.11.1, have duration 2Δ , that is, twice as long as the pulse case. The linear combination of (24.11.1) is equivalent to connecting the sample values I_m by straight line segments.

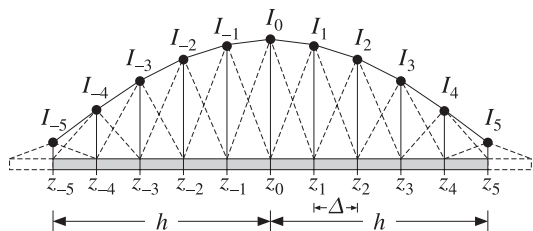


Fig. 24.11.1 Triangular basis functions with $N = 11, M = 5$.

The antenna is divided into $N = 2M$ segments of width $\Delta = l/2M = h/M$, and the $(2M + 1)$ points $z_m = m\Delta, -M \leq m \leq M$, lie at the end points of these segments. As depicted in Fig. 24.11.1, the influence of the last current sample I_M at z_M (and I_{-M} at z_{-M}) may be thought of as extending beyond the end of the antenna by an additional segment. The vanishing of the current at the ends of the antenna is enforced by the conditions $I_M = I_{-M} = 0$.

For point-matching, the Hallén impedance matrix (24.8.9) will be given as follows:

$$\begin{aligned} Z_{nm} &= \frac{j\eta}{2\pi} \int_{-h}^h G(z_n - z') B(z' - z_m) dz' \\ &= \frac{j\eta}{2\pi} \int_{z_m - \Delta}^{z_m + \Delta} \left(1 - \frac{|z' - z_m|}{\Delta}\right) G(z_n - z') dz' \\ &= \frac{j\eta}{2\pi} \int_{-\Delta}^{\Delta} \left(1 - \frac{|z|}{\Delta}\right) G(z_n - z_m - z) dz \end{aligned} \quad (24.11.3)$$

which differs by a factor of Δ from the Galerkin case of the pulse basis, Eq. (24.10.4). The Hallén matrix equation remains the same as (24.9.4):

$$Z\mathbf{I} = \mathbf{v} = C_1\mathbf{c} + V_0\mathbf{s} \quad (24.11.4)$$

with the same right-hand vectors, that is, $c_n = \cos kz_n$ and $s_n = \sin k|z_n|, -M \leq n \leq M$. It may be solved by the function `hmat`, called with the option, `basis='t'`. A 32-point Gauss-Legendre quadrature is used to compute the integrals in (24.11.3).

The exact and approximate kernel current solutions and input admittance exhibit the same behavior in the triangular basis as in the pulse basis.

Using the exact kernel, the triangular basis converges faster than the pulse basis as the number of segments M increases. Fig. 24.11.2 compares the convergence of the input admittance of a half-wave dipole with radius $a = 0.005\lambda$ for the two bases.

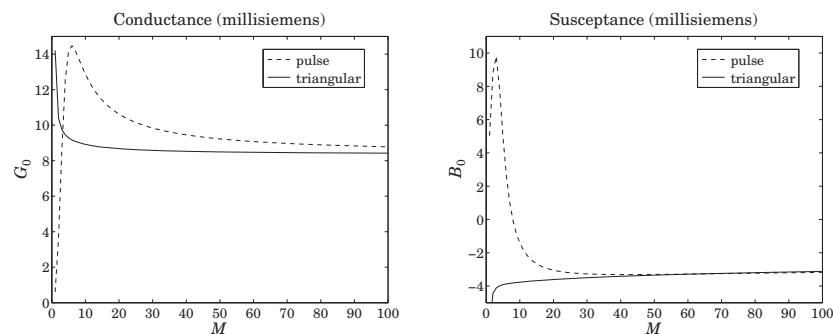


Fig. 24.11.2 Input admittance computed with pulse and triangular basis functions.

24.12 NEC Sinusoidal Basis

The Numerical Electromagnetics Code (NEC) is a widely used public-domain program for modeling antennas and other structures [1748]. The program solves Pocklington's equation using point-matching and a spline-like sinusoidal basis. A similar basis was originally used by [1732]. For a linear antenna, the basis is defined by:

$$B(z) = \begin{cases} A_- + B_- \sin k(z + \Delta) + C_- \cos k(z + \Delta), & -\frac{3\Delta}{2} \leq z \leq -\frac{\Delta}{2} \\ A_0 + B_0 \sin kz + C_0 \cos kz, & -\frac{\Delta}{2} \leq z \leq \frac{\Delta}{2} \\ A_+ + B_+ \sin k(z - \Delta) + C_+ \cos k(z - \Delta), & \frac{\Delta}{2} \leq z \leq \frac{3\Delta}{2} \end{cases} \quad (24.12.1)$$

where Δ is the segment length defined as usual by $\Delta = 2h / (2M + 1)$. The basis function $B(z)$ is shown on the left of Fig. 24.12.1. It extends over three consecutive segments.

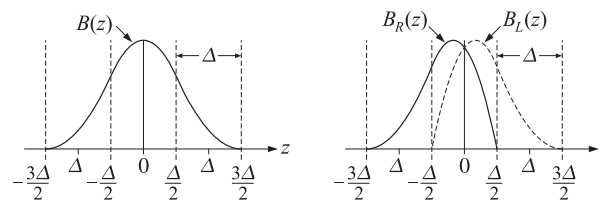


Fig. 24.12.1 NEC sinusoidal basis functions.

The A, B, C coefficients are determined by imposing the spline-like conditions that (a) the three pieces of $B(z)$ join continuously, as do their slopes, at the points $z = \pm\Delta/2$, (b) at the end-points $z = \pm 3\Delta/2$, the function $B(z)$ and its derivative vanish, and (c) at the center $z = 0$, $B(0)$ is normalized to one. These conditions provide nine equations

for the nine coefficients, with solution:

$$A_0 = \frac{1 - 2c_\Delta^2}{1 + c_\Delta - 2c_\Delta^2}, \quad B_0 = 0, \quad C_0 = \frac{c_\Delta}{1 + c_\Delta - 2c_\Delta^2} \quad (24.12.2)$$

$$A_\pm = \frac{1}{2(1 + c_\Delta - 2c_\Delta^2)}, \quad B_\pm = \mp \frac{s_\Delta}{2(1 + c_\Delta - 2c_\Delta^2)}, \quad C_\pm = -\frac{c_\Delta}{2(1 + c_\Delta - 2c_\Delta^2)} \quad (24.12.3)$$

where c_Δ, s_Δ are shorthands for the quantities:

$$c_\Delta = \cos\left(\frac{k\Delta}{2}\right), \quad s_\Delta = \sin\left(\frac{k\Delta}{2}\right) \quad (24.12.4)$$

The current expansion in terms of this basis is as follows:

$$I(z) = \sum_{m=-M}^M b_m B(z - z_m) \quad (24.12.5)$$

where $z_m = m\Delta$, $-M \leq m \leq M$ and the coefficients b_m are to be determined.

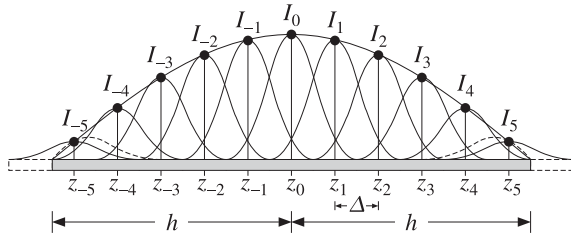


Fig. 24.12.2 NEC sinusoidal basis with $N = 11, M = 5$.

Fig. 24.12.2 depicts (24.12.5). Actually, the NEC basis handles the two end segments centered at $z_{\pm M}$ separately [1748] and uses the following expansion instead of (24.12.5):

$$I(z) = b_{-M} B_L(z - z_{-M}) + \sum_{m=-(M-1)}^{(M-1)} b_m B(z - z_m) + b_M B_R(z - z_M) \quad (24.12.6)$$

where $B_R(z)$ and $B_L(z)$ are given by:

$$B_R(z) = \begin{cases} A_-^R + B_-^R \sin k(z + \Delta) + C_-^R \cos k(z + \Delta), & -\frac{3\Delta}{2} \leq z \leq -\frac{\Delta}{2} \\ A_0^R + B_0^R \sin kz + C_0^R \cos kz, & -\frac{\Delta}{2} \leq z \leq \frac{\Delta}{2} \end{cases} \quad (24.12.7)$$

and $B_L(z) = B_R(-z)$, where the coefficients are determined by requiring (a) the continuity of the two pieces and their derivatives at $z = -\Delta/2$, (b) the vanishing of $B_R(z)$ at $z = \Delta/2$, (c) the vanishing of $B_R(z)$ and its derivative at $z = -3\Delta/2$, and (d) the normalization condition $B_R(0) = 1$. These give:

$$\begin{aligned} A_-^R &= \frac{1}{1 + 3c_\Delta - 4c_\Delta^2}, & B_-^R &= \frac{s_\Delta}{1 + 3c_\Delta - 4c_\Delta^2}, & C_-^R &= -\frac{c_\Delta}{1 + 3c_\Delta - 4c_\Delta^2} \\ A_0^R &= \frac{1 - 4c_\Delta^2}{1 + 3c_\Delta - 4c_\Delta^2}, & B_0^R &= -\frac{s_\Delta}{1 + 3c_\Delta - 4c_\Delta^2}, & C_0^R &= \frac{3c_\Delta}{1 + 3c_\Delta - 4c_\Delta^2} \end{aligned} \quad (24.12.8)$$

The functions $B_L(z)$ and $B_R(z)$ are depicted on the right of Fig. 24.12.1, and are shown as dashed curves at the antenna ends in Fig. 24.12.2. Because of the end conditions $I_{\pm M} = 0$, it makes very little difference whether one uses (24.12.5) or (24.12.6). We will use the former.

Because $B(z)$ straddles three adjacent segments and $B(\pm\Delta) \neq 0$, the value of the current at a sample point z_n will receive contributions from the two adjacent samples z_{n-1} and z_{n+1} . For $-M < n < M$, we have from (24.12.5):

$$\begin{aligned} I_n = I(z_n) &= b_{n-1} B(z_n - z_{n-1}) + b_n B(z_n - z_n) + b_{n+1} B(z_n - z_{n+1}) \\ &= b_{n-1} B(\Delta) + b_n B(0) + b_{n+1} B(-\Delta) \end{aligned}$$

or, noting that $B(0) = 1$ and defining $\beta = B(\Delta) = B(-\Delta)$,

$$I_n = \beta b_{n-1} + b_n + \beta b_{n+1}, \quad -M < n < M \quad (24.12.9)$$

and for the end points:

$$I_{-M} = b_{-M} + \beta b_{-M+1}, \quad I_M = \beta b_{M-1} + b_M \quad (24.12.10)$$

Eqs. (24.12.9) and (24.12.10) can be arranged into a tridiagonal matrix, for example,

$$I = \begin{bmatrix} I_{-3} \\ I_{-2} \\ I_{-1} \\ I_0 \\ I_1 \\ I_2 \\ I_3 \end{bmatrix} = \begin{bmatrix} 1 & \beta & 0 & 0 & 0 & 0 & 0 \\ \beta & 1 & \beta & 0 & 0 & 0 & 0 \\ 0 & \beta & 1 & \beta & 0 & 0 & 0 \\ 0 & 0 & \beta & 1 & \beta & 0 & 0 \\ 0 & 0 & 0 & \beta & 1 & \beta & 0 \\ 0 & 0 & 0 & 0 & \beta & 1 & \beta \\ 0 & 0 & 0 & 0 & 0 & \beta & 1 \end{bmatrix} \begin{bmatrix} b_{-3} \\ b_{-2} \\ b_{-1} \\ b_0 \\ b_1 \\ b_2 \\ b_3 \end{bmatrix} \equiv \mathcal{B} \mathbf{b} \quad (24.12.11)$$

It follows from Eq. (24.12.1) that the parameter β is equal to $A_+ + C_+$, or,

$$\beta = B(\Delta) = \frac{1 - c_\Delta}{2(1 + c_\Delta - 2c_\Delta^2)} \quad (24.12.12)$$

For the pulse and triangular bases, the matrix \mathcal{B} is equal to the identity matrix because in these cases $\beta = B(\Delta) = 0$.

Next, we determine the solution of Hallén's equation with point matching. Inserting the expansion (24.12.5) into (24.8.1), and evaluating it at the sample point z_n , we obtain the matrix equation for the coefficients b_m :

$$\sum_{m=-M}^M Z_{nm} b_m = C_1 \cos kz_n + V_0 \sin k|z_n|, \quad -M \leq n \leq M \quad (24.12.13)$$

or, written compactly,

$$\mathcal{Z} \mathbf{b} = C_1 \mathbf{c} + V_0 \mathbf{s} \quad (24.12.14)$$

where the matrix elements Z_{nm} are given by:

$$\begin{aligned} Z_{nm} &= \frac{j\eta}{2\pi} \int_{-h}^h G(z_n - z') B(z' - z_m) dz' \\ &= \frac{j\eta}{2\pi} \int_{-3\Delta/2}^{3\Delta/2} B(z) G(z_n - z_m - z) dy \end{aligned} \quad (24.12.15)$$

Substituting (24.12.11) into (24.12.14), we obtain,

$$ZB^{-1}I = C_1c + V_0s \tag{24.12.16}$$

This has the same form as (24.9.4) with the replacement $Z \rightarrow ZB^{-1}$ and therefore, it can be solved by the same method. The MATLAB function `hdelta` implements the solution with the option, `basis='n'`.

The function `hmat` calculates Z , and it also optionally, outputs the matrix B , which is required in (24.12.16). The integral in (24.12.15) is calculated with Gauss-Legendre quadrature. The basis function $B(z)$ may be evaluated with the help of the MATLAB function `hbasis`, with usage:

```
B = hbasis(z,Delta,basis); % evaluate basis function B(z) at a vector of z's
```

where `Delta` is the value of Δ and the string `basis` can take the possible values 'p', 't', 'n', 'nr', 'nl', for pulse, triangular, and NEC basis (the last two options evaluate the rightmost and leftmost NEC basis functions.)

The NEC basis for the Hallén equation has very comparable performance to the pulse basis with point matching—the two agreeing to within one percent or so, and hence, we do not give any further examples.

24.13 Hallén's Equation for Arbitrary Incident Field

Here, we discuss the solution of Hallén's equation (24.3.11) with arbitrary incident field:

$$\frac{j\eta}{2\pi} \int_{-h}^h G(z-z')I(z')dz' = C_1e^{jkz} + C_2e^{-jkz} + \int_{-h}^h F(z-z')E_{in}(z')dz' \tag{24.13.1}$$

In applying the method of moments, we expand the current and the incident field with respect to a given basis $B(z)$:

$$I(z') = \sum_{m=-M}^M I_m B(z' - z_m) \tag{24.13.2}$$

$$E_{in}(z') = \sum_{m=-M}^M E_m B(z' - z_m)$$

We consider only the point-matching case. Sampled at the points $z_n = n\Delta z$, the convolution of the incident field with the Green's function $F(z)$ becomes:

$$\int_{-h}^h F(z_n - z')E_{in}(z')dz' = \sum_{m=-M}^M E_m \int_{-h}^h F(z_n - z')B(z' - z_m)dz'$$

We define the Green's matrix F_{nm} , for $-M \leq n, m \leq M$ by

$$F_{nm} = \int_{-h}^h F(z_n - z')B(z' - z_m)dz' = \int_{-h}^h F(z_n - z_m - z)B(z)dz \tag{24.13.3}$$

It follows that the discretized Hallén equation (24.13.1) takes the form:

$$\sum_{m=-M}^M Z_{nm}I_m = C_1e^{jkz_n} + C_2e^{-jkz_n} + \sum_{m=-M}^M F_{nm}E_m \tag{24.13.4}$$

where Z_{nm} are defined as in the previous sections:

$$Z_{nm} = \int_{-h}^h G(z_n - z')B(z' - z_m)dz' = \int_{-h}^h G(z_n - z_m - z)B(z)dz$$

Eq. (24.13.4) can be written in the compact form:

$$ZI = C_1s_1 + C_2s_2 + FE \tag{24.13.5}$$

where s_1 and s_2 are column vectors with elements $s_1(n) = e^{jkz_n}$ and $s_2(n) = e^{-jkz_n}$. Defining the $N \times 2$ matrix $S = [s_1, s_2]$ and the two-dimensional column vector of constants $C = [C_1, C_2]^T$, we write Eq. (24.13.5) in the form:

$$ZI = SC + FE \tag{24.13.6}$$

For the NEC basis, the expansion (24.13.2) has the modified form:

$$I(z') = \sum_{m=-M}^M b_m B(z' - z_m), \quad E_{in}(z') = \sum_{m=-M}^M e_m B(z' - z_m) \tag{24.13.7}$$

where the vectors of the coefficients b_m and e_m are related to the values of the current and field, I_m and E_m , at the sample points z_m via the tridiagonal matrix B of (24.12.11):

$$I = Bb, \quad E = Be \tag{24.13.8}$$

The discretized Hallén equation now takes the form:

$$Zb = SC + Fe \tag{24.13.9}$$

and expressed in terms of I and E :

$$ZB^{-1}I = SC + FB^{-1}E \tag{24.13.10}$$

For the pulse, triangular, and delta bases B is replaced by the identity matrix. It is not possible to wrap this equation in half because E is not necessarily symmetric about its middle. The constants C must be found by imposing the two independent end conditions $I(z_M) = I(-z_M) = 0$. These conditions can be written compactly as:

$$U^T I = 0$$

where $U = [u_{top}, u_{bot}]$ and $u_{top} = [1, 0, \dots, 0]^T$ selects the top entry of the vector I , while $u_{bot} = [0, \dots, 0, 1]^T$ selects the bottom entry. Solving for I , we have:

$$I = BZ^{-1}SC + BZ^{-1}FB^{-1}E \tag{24.13.11}$$

Multiplying from the left by the matrix U^T , we obtain the condition:

$$U^T \mathbf{I} = U^T \mathcal{B} \mathcal{Z}^{-1} S \mathbf{C} + U^T \mathcal{B} \mathcal{Z}^{-1} F \mathcal{B}^{-1} \mathbf{E} = 0$$

which may be solved for \mathbf{C} :

$$\mathbf{C} = - (U^T \mathcal{B} \mathcal{Z}^{-1} S)^{-1} (U^T \mathcal{B} \mathcal{Z}^{-1} F \mathcal{B}^{-1} \mathbf{E}) \quad (24.13.12)$$

Eqs. (24.13.11) and (24.13.12) describe the complete solution of the discrete Hallén equation (24.13.10). The MATLAB function `hfield` implements the solution, with usage:

```
[I,z,cnd] = hfield(L,a,E,ker,basis); % Hallen's equation with arbitrary incident E-field
```

where instead of the parameter M , it has as input the vector \mathbf{E} of the samples of the incident field. The dimension $N = 2M + 1$ is extracted from the length of \mathbf{E} . The strings `ker` and `basis` have the same meaning as for the function `hdelta`.

The functions `hdelta` and `hfield` produce practically identical output in the delta-gap case, that is, when the incident field is:

$$\mathbf{E} = \underbrace{[0, 0, \dots, 0]}_{M \text{ zeros}}, \frac{1}{\Delta}, \underbrace{[0, \dots, 0, 0]}_{M \text{ zeros}}^T \quad (24.13.13)$$

The middle entry imitates the delta-gap $V_0 \delta(z) \approx V_0 / \Delta$ near $z = 0$. For the case of a field incident at a polar angle θ as in Eq. (24.2.4), the sampled vector \mathbf{E} will have entries:

$$E_n = E_0 \sin \theta e^{jkz_n \cos \theta}, \quad z_n = n\Delta, \quad -M \leq n \leq M \quad (24.13.14)$$

Fig. 24.13.1 compares the current solutions using `hdelta` and `hfield` with the input of Eq. (24.13.13), for the case of a half-wave dipole of radius $a = 0.005\lambda$, using a pulse basis with $M = 50$ and the exact kernel.

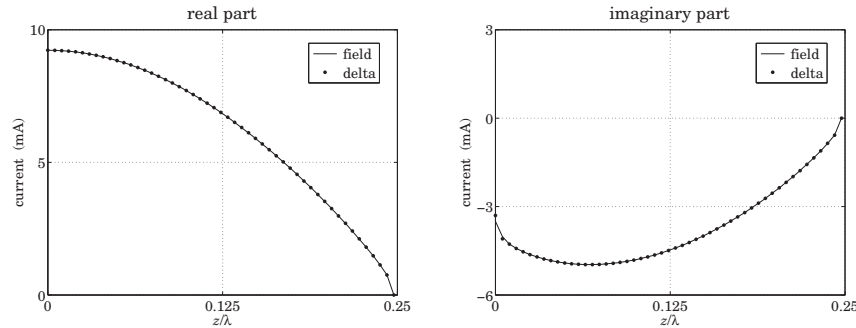


Fig. 24.13.1 Comparison of delta-gap and field solutions for a half-wave dipole.

For larger values of M , the results of the two methods are indistinguishable. The following example MATLAB code can be used to generate these graphs:

```
L=0.5; a=0.005; M = 30; D = L/(2*M+1);
E = zeros(2*M+1,1); E(M+1)=1/D; % define E by Eq. (24.13.13)

[I,f,z] = hfield(L,a,E,'e','p'); % field input
[Id,z] = hdelta(L,a,M,'e','p'); % delta-gap input

figure; plot(z,real(I*f),'-', z,real(Id),'-.');
figure; plot(z,imag(I*f),'-', z,imag(Id),'-.');
```

Next, we discuss the computation of the matrix elements F_{nm} for different basis functions. It follows from Eq. (24.13.3) and the even-ness of $B(z)$ that F_{nm} is a Toeplitz and symmetric matrix and, therefore, it depends on n, m through the difference $|n - m|$. Thus, it can be constructed by $F_{nm} = f_{|n-m|}$, where f_m is given by

$$f_m = \int_{-h}^h F(m\Delta - z) B(z) dz, \quad m = 0, 1, \dots, 2M \quad (24.13.15)$$

Once the vector $\mathbf{f} = [f_0, f_1, \dots, f_{2M}]$ is computed, the matrix F can be constructed as a Toeplitz matrix whose first row or first column is \mathbf{f} , by calling the function `toeplitz`:

$$F = \text{toeplitz}(\mathbf{f}, \mathbf{f})$$

For the Green's function $F(z)$ we choose,

$$F(z) = \sin k|z|$$

although any of those listed in Eq. (24.3.8) could have been chosen. The integrals in (24.13.15) can be done in closed form resulting in the following expressions for f_m in the various bases. For the *delta-function* basis $B(z) = \delta(z) \Delta$, we have:

$$f_m = F(m\Delta) \Delta = \sin(km\Delta) \Delta, \quad 0 \leq m \leq 2M \quad (24.13.16)$$

For the *pulse* basis, f_m is given by

$$f_m = \int_{-\Delta/2}^{\Delta/2} \sin(k|m\Delta - z|) dz \quad (24.13.17)$$

which gives:

$$f_m = \frac{2}{k} \sin\left(\frac{k\Delta}{2}\right) \sin(km\Delta), \quad 1 \leq m \leq 2M$$

$$f_0 = \frac{2}{k} \left(1 - \cos \frac{k\Delta}{2}\right) \quad (24.13.18)$$

For the *triangular* basis, we have:

$$f_m = \int_{-\Delta}^{\Delta} \left(1 - \frac{|z|}{\Delta}\right) \sin(k|m\Delta - z|) dz$$

with the result:

$$f_m = \frac{2(1 - \cos k\Delta)}{k^2 \Delta} \sin(km\Delta), \quad 1 \leq m \leq 2M$$

$$f_0 = \frac{2(k\Delta - \sin k\Delta)}{k^2 \Delta} \quad (24.13.19)$$

For the NEC basis, f_m is defined by

$$f_m = \int_{-3\Delta/2}^{3\Delta/2} B(z) \sin(k|m\Delta - z|) dz$$

where $B(z)$ is given by (24.12.1), and we obtain:

$$\begin{aligned} f_m &= \frac{\Delta}{2D} \left(\cos \frac{k\Delta}{2} - \cos \frac{3k\Delta}{2} \right) \sin(km\Delta), \quad 2 \leq m \leq 2M \\ f_0 &= \frac{2}{kD} \left[\cos \frac{k\Delta}{2} - \cos k\Delta + \frac{k\Delta}{4} \sin \frac{3k\Delta}{2} \right] \\ f_1 &= \frac{1}{kD} \left[1 - \cos \frac{k\Delta}{2} + \frac{k\Delta}{4} \left(\sin \frac{k\Delta}{2} + \sin \frac{3k\Delta}{2} - \sin \frac{5k\Delta}{2} \right) \right] \end{aligned} \quad (24.13.20)$$

where D is the normalization factor:

$$D = 1 + \cos \frac{k\Delta}{2} - 2 \cos^2 \frac{k\Delta}{2} = \cos \frac{k\Delta}{2} - \cos k\Delta$$

As in the delta-gap case, the pulse and NEC bases give almost identical results, while the triangular basis converges the fastest. For large M , all bases produce virtually the same result if the exact kernel is used. The approximate kernel solutions suffer from the same type of oscillations as in the delta-gap case.

Fig. 24.13.2 shows the current induced on a half-wave dipole antenna of radius $a = 0.005\lambda$ by a plane wave incident from broadside. Setting $\theta = 90^\circ$ in (24.13.14) results into constant E -field samples $E_m = E_0$, for $-M \leq m \leq M$. To illustrate the convergence properties, the current was computed using a triangular basis with $M = 30$, and then using a pulse basis with successively increasing values of $M = 30, 50, 100$, converging to the triangular case. The $M = 50, 100$ cases for a triangular basis are not shown because they are indistinguishable from the $M = 30$ case.

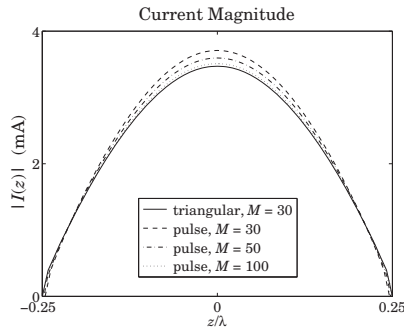


Fig. 24.13.2 Current on half-wave dipole induced by plane wave incident from broadside.

24.14 Solving Pocklington's Equation

In this section, we discuss the numerical solution of Pocklington's equation (24.1.9) for arbitrary incident field. Rearranging some constants, we can write it in the form:

$$(\partial_z^2 + k^2) \frac{j\eta}{2\pi} \int_{-h}^h G(z-z') I(z') dz' = 2kE_{in}(z) \quad (24.14.1)$$

where $G(z)$ is the exact or the approximate kernel. Eq. (24.14.1) must be solved subject to the end-point conditions $I(\pm h) = 0$. Its numerical solution has been studied extensively [1725-1785].

In our method of solution we use point matching and, following Ref. [1747], apply a finite-difference approximation to the Helmholtz operator $(\partial_z^2 + k^2)$ to convert (24.14.1) into a matrix equation for the current. The method generates essentially the same solutions as the Hallén equation and is efficiently implementable, making use of the numerical tools that we developed in the previous sections for computing the Hallén impedance matrix for different bases,

$$Z_{nm} = \frac{j\eta}{2\pi} \int_{-h}^h G(z_n - z_m - z) B(z) dz \quad (24.14.2)$$

For convenience, we write (24.14.1) in the form:

$$(\partial_z^2 + k^2) V(z) = 2kE_{in}(z), \quad V(z) = \frac{j\eta}{2\pi} \int_{-h}^h G(z-z') I(z') dz' \quad (24.14.3)$$

Evaluating (24.14.3) at the $N = 2M + 1$ sample points $z_n = n\Delta$, $-M \leq n \leq M$, where the spacing Δ is given by $\Delta = 2h/(2M + 1)$ in the pulse, NEC, and delta-function bases, and $\Delta = h/M$ in the triangular basis, we have:

$$(\partial_z^2 + k^2) V(z_n) = 2kE_{in}(z_n), \quad V(z_n) = \frac{j\eta}{2\pi} \int_{-h}^h G(z_n - z') I(z') dz' \quad (24.14.4)$$

Following [1747], we replace the second derivative in z by the finite difference:

$$\partial_z^2 V(z_n) \approx \frac{V(z_{n+1}) - 2V(z_n) + V(z_{n-1}))}{\Delta^2}$$

Denoting $V_n = V(z_n)$ and $E_n = E_{in}(z_n)$, Eq. (24.14.4) becomes:

$$\frac{V_{n+1} - 2V_n + V_{n-1}}{\Delta^2} + k^2 V_n = 2kE_n$$

which can be re-written as:

$$V_{n+1} - 2\alpha V_n + V_{n-1} = E_n d \quad (24.14.5)$$

where we defined $\alpha = 1 - k^2\Delta^2/2$ and $d = 2k\Delta^2$, and we must restrict n to the range $-(M - 1) \leq n \leq M - 1$. Eq. (24.14.5) may be written in the following tridiagonal matrix

form that displays *all* the samples V_n and E_n , $-M \leq n \leq M$, shown here for $M = 3$:

$$\begin{bmatrix} 0 & 0 & 0 & 0 & 0 & 0 & 0 \\ 1 & -2\alpha & 1 & 0 & 0 & 0 & 0 \\ 0 & 1 & -2\alpha & 1 & 0 & 0 & 0 \\ 0 & 0 & 1 & -2\alpha & 1 & 0 & 0 \\ 0 & 0 & 0 & 1 & -2\alpha & 1 & 0 \\ 0 & 0 & 0 & 0 & 1 & -2\alpha & 1 \\ 0 & 0 & 0 & 0 & 0 & 0 & 0 \end{bmatrix} \begin{bmatrix} V_{-3} \\ V_{-2} \\ V_{-1} \\ V_0 \\ V_1 \\ V_2 \\ V_3 \end{bmatrix} = \begin{bmatrix} 0 & 0 & 0 & 0 & 0 & 0 & 0 \\ 0 & 1 & 0 & 0 & 0 & 0 & 0 \\ 0 & 0 & 1 & 0 & 0 & 0 & 0 \\ 0 & 0 & 0 & 1 & 0 & 0 & 0 \\ 0 & 0 & 0 & 0 & 1 & 0 & 0 \\ 0 & 0 & 0 & 0 & 0 & 1 & 0 \\ 0 & 0 & 0 & 0 & 0 & 0 & 0 \end{bmatrix} \begin{bmatrix} E_{-3} \\ E_{-2} \\ E_{-1} \\ E_0 \\ E_1 \\ E_2 \\ E_3 \end{bmatrix} d \quad (24.14.6)$$

where the top and bottom rows of zeros are redundant and have been added to make these matrices square, both having rank $(N - 2)$. We may write (24.14.6) compactly as:

$$\mathcal{A}V = QEd \quad (24.14.7)$$

We note that Q is a projection matrix and so is its complement $\mathcal{P} = I - Q$,[†] which enforces the end-point conditions $I_{\pm M} = 0$:

$$\mathcal{P}I = (I - Q)I = \begin{bmatrix} 1 & 0 & 0 & 0 & 0 & 0 & 0 \\ 0 & 0 & 0 & 0 & 0 & 0 & 0 \\ 0 & 0 & 0 & 0 & 0 & 0 & 0 \\ 0 & 0 & 0 & 0 & 0 & 0 & 0 \\ 0 & 0 & 0 & 0 & 0 & 0 & 0 \\ 0 & 0 & 0 & 0 & 0 & 0 & 0 \\ 0 & 0 & 0 & 0 & 0 & 0 & 1 \end{bmatrix} \begin{bmatrix} I_{-3} \\ I_{-2} \\ I_{-1} \\ I_0 \\ I_1 \\ I_2 \\ I_3 \end{bmatrix} = \begin{bmatrix} I_{-3} \\ 0 \\ 0 \\ 0 \\ 0 \\ 0 \\ I_3 \end{bmatrix} = 0 \quad (24.14.8)$$

The samples V_n can be represented in terms of the Hallén impedance matrix and current samples I_n with respect to a particular basis $B(z)$. Inserting the expansion,

$$I(z) = \sum_{m=-M}^M I_m B(z - z_m)$$

into (24.14.4), we have:

$$V_n = \sum_{m=-M}^M I_m \frac{j\eta}{2\pi} \int_{-h}^h G(z_n - z_m - z) B(z) dz = \sum_{m=-M}^M Z_{nm} I_m$$

with Z_{nm} given by (24.14.2). Vectorially, we may write

$$V = ZI$$

For the NEC basis, we have instead:

$$I(z) = \sum_{m=-M}^M b_m B(z - z_m), \quad \text{and,}$$

$$V_n = \sum_{m=-M}^M b_m \frac{j\eta}{2\pi} \int_{-h}^h G(z_n - z_m - z) B(z) dz = \sum_{m=-M}^M Z_{nm} b_m, \quad \text{or,}$$

[†]here, I is the identity matrix.

$$V = Zb, \quad \text{with } I = Bb \Rightarrow V = ZB^{-1}I \quad (24.14.9)$$

with B defined as in (24.12.11). Combining with (24.14.7), we obtain:

$$\mathcal{A}ZB^{-1}I = QEd \quad (24.14.10)$$

Using (24.14.8) and the idempotent property $Q^2 = Q$, we have $I = QI = Q^2I$. Making this replacement into (24.14.10), we obtain:

$$\boxed{(\mathcal{A}ZB^{-1}Q)(QI) = (QE)d} \quad (24.14.11)$$

This is the discretized Pocklington equation for the current. The operation $\mathcal{A}ZB^{-1}Q$ simply extracts the middle portion of the matrix $\mathcal{A}ZB^{-1}$, and QI and QE extract the middle portions of I and E . Indeed, we have

$$QE = \begin{bmatrix} 0 & 0 & 0 & 0 & 0 & 0 & 0 \\ 0 & 1 & 0 & 0 & 0 & 0 & 0 \\ 0 & 0 & 1 & 0 & 0 & 0 & 0 \\ 0 & 0 & 0 & 1 & 0 & 0 & 0 \\ 0 & 0 & 0 & 0 & 1 & 0 & 0 \\ 0 & 0 & 0 & 0 & 0 & 1 & 0 \\ 0 & 0 & 0 & 0 & 0 & 0 & 0 \end{bmatrix} \begin{bmatrix} E_{-3} \\ E_{-2} \\ E_{-1} \\ E_0 \\ E_1 \\ E_2 \\ E_3 \end{bmatrix} = \begin{bmatrix} 0 \\ E_{-2} \\ E_{-1} \\ E_0 \\ E_1 \\ E_2 \\ 0 \end{bmatrix} \equiv \begin{bmatrix} 0 \\ \bar{E} \\ 0 \end{bmatrix}$$

and similarly, $\mathcal{A}ZB^{-1}$ and $\mathcal{A}ZB^{-1}Q$ have the structures:

$$\mathcal{A}ZB^{-1} = \begin{bmatrix} 0 & \mathbf{0}^T & 0 \\ \mathbf{a} & \tilde{Z} & \mathbf{b} \\ 0 & \mathbf{0}^T & 0 \end{bmatrix} \Rightarrow \mathcal{A}ZB^{-1}Q = \begin{bmatrix} 0 & \mathbf{0}^T & 0 \\ \mathbf{0} & \tilde{Z} & \mathbf{0} \\ 0 & \mathbf{0}^T & 0 \end{bmatrix}$$

where \tilde{Z} is an $(N-2) \times (N-2)$ non-singular matrix. Thus, (24.14.11) is equivalent to:

$$\begin{bmatrix} 0 & \mathbf{0}^T & 0 \\ \mathbf{0} & \tilde{Z} & \mathbf{0} \\ 0 & \mathbf{0}^T & 0 \end{bmatrix} \begin{bmatrix} 0 \\ \bar{I} \\ 0 \end{bmatrix} = \begin{bmatrix} 0 \\ \bar{E} \\ 0 \end{bmatrix} d \Rightarrow \tilde{Z}\bar{I} = \bar{E}d \quad (24.14.12)$$

with solution:

$$\boxed{\bar{I} = \tilde{Z}^{-1}\bar{E}d}, \quad I = QI = \begin{bmatrix} 0 \\ \bar{I} \\ 0 \end{bmatrix} \quad (24.14.13)$$

The MATLAB function `pfield` implements the above solution procedure:

```
[I,z,cnd] = pfield(L,a,E,ker,basis); solve Pocklington's equation
```

where I, E, z are the vectors of sampled values $I_n, E_n, z_n = n\Delta$, the quantity `cnd` is the condition number of the Pocklington impedance matrix \tilde{Z} , and the string constants `ker` and `basis` take the possible values:

```
ker = 'e', 'a', % exact or approximate kernel
basis = 'p', 't', 'n', 'd', % pulse, triangular, NEC, or delta-function basis
```

The condition number of the Pocklington matrix \tilde{Z} can be one or more orders of magnitude larger than that of the Hallén matrix Z . Yet, the computed currents by the functions `pfieid` and `hfieid` are remarkably close to each other and virtually indistinguishable over a wide range of the parameters L, a, M .

The large condition number is due to the Helmholtz operator $(\partial_z^2 + k^2)$ —represented in discrete form by the matrix \mathcal{A} —which causes the Pocklington kernel to become less well-behaved than the Hallén kernel. This has been a primary concern in all the numerical methods for solving Pocklington's equation.

Fig. 24.14.1 shows the currents computed by the Pocklington and Hallén methods induced on a half-wave dipole antenna of radius $a = 0.005\lambda$ by a plane wave incident from broadside (left graph) and by a delta-gap input (right graph).

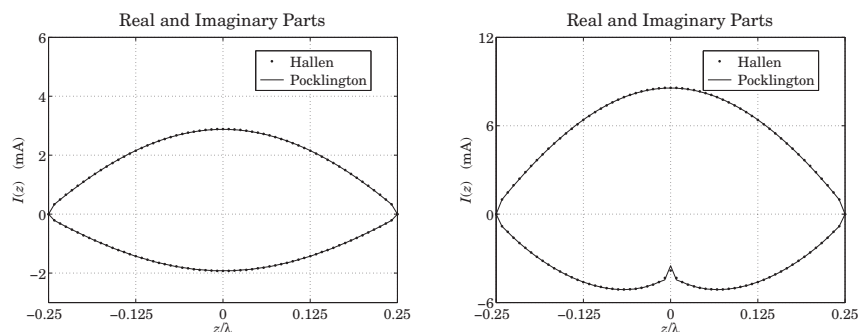


Fig. 24.14.1 Comparison of Pocklington and Hallén equation solutions.

The top curves represent the real parts of the currents and the bottom ones, the imaginary parts. We used a triangular basis with the exact kernel and $M = 30$ segments. The condition numbers of the impedance matrices Z and \tilde{Z} were 17 and 377, respectively. The following MATLAB code illustrates the computation:

```
L = 0.5; a = 0.005; M = 30; ker = 'e'; basis = 't';
if basis=='t', D = L/(2*M); else D = L/(2*M+1); end

E = zeros(2*M+1,1); E(M+1) = 1/D;           % delta-gap input
% E = ones(2*M+1,1);                          % plane-wave input

[If,zf,cf] = hfieid(L,a,E,ker,basis);         % Hallén
[Ip,zp,cp] = pfieid(L,a,E,ker,basis);         % Pocklington

plot(zf,real(If),'.', zp, real(Ip), '-.', zf,imag(If),'.', zp, imag(Ip), '-');
```

To see the dramatic difference between the Hallén and Pocklington impedance matrices Z and \tilde{Z} , Fig. 24.14.2 plots the singular values of these matrices (normalized to their maximum value) for the case of a half-wave dipole of radius $a = 0.005\lambda$ using a triangular basis with $M = 100$ and the exact kernel. The computed condition numbers for Z and \tilde{Z} were 59 and 1185, respectively.

The numerical solution of Pocklington's equation has similar properties as the Hallén case, such as, the triangular basis converging faster than the other bases with increasing

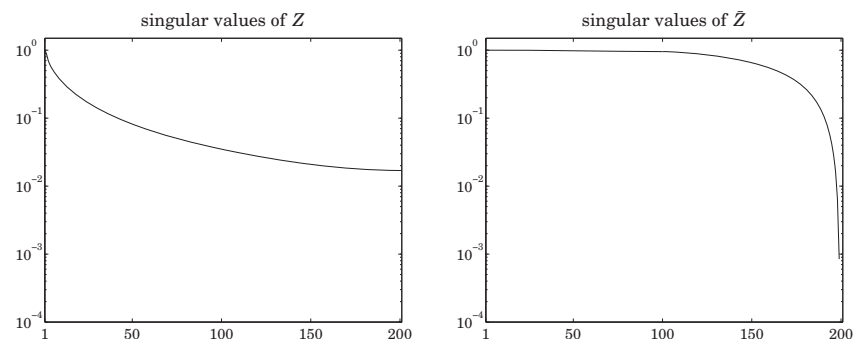


Fig. 24.14.2 Singular values of the impedance matrices Z and \tilde{Z} for $N=2M+1=201$.

M , and the use of the approximate kernel causing oscillations at the end-points of the antenna (and at the center for delta-gap input.)

This chapter dealt with the currents on a single linear antenna. The case of several antennas forming an array and interacting with each other is treated in Chap. 25.

Hallén's and Pocklington's integral equations generalize into a system of several coupled integral equations for the currents on the antennas. We solve the coupled Hallén equations in the case of delta-gap center-driven antennas. The linearity of the equations allows us to collect them together into a block matrix system from which the currents on each antenna can be obtained.

One simplification arises in the case of an array of identical antennas. Then, the block linear system can be wrapped in half much like it was done in Sec. 24.9, thus, reducing the computational cost.

The case of an array of non-identical antennas is also considered and we obtain solutions for Yagi-Uda arrays with parasitic reflector and director antennas.

24.15 Problems

24.1 Plot the approximations of $\sin kR/kR$ given in Eqs. (24.6.1) and (24.6.18) versus R in the range $R \leq 2\lambda$ and verify their validity. Prove the identity:

$$\frac{\sin kR}{kR} = \frac{\sin(kR/8)}{kR/8} \cos(kR/8) \cos(kR/4) \cos(kR/2)$$

which leads to the approximation:

$$\frac{\sin kR}{kR} \approx \cos(kR/8) \cos(kR/4) \cos(kR/2)$$

Determine the range of applicability of this approximation and plot it together with the previous two cases. Show that it leads to a six-term sinusoidal fit for the current. What are the current basis functions $I_i(z)$, $i = 1, 2, \dots, 6$, in this case?

24.2 Computer Experiment—Solving Hallén's Equation. Consider a dipole antenna of length $l = 0.5\lambda$ and radius $a = 0.005\lambda$.

- a. For each of the values $M = 20, 50, 100, 200$, solve Hallén's equation for a delta-gap input with voltage $V_0 = 1$ volt using both the exact and the approximate kernels. Plot the real and imaginary parts of the current $I_m = I(z_m)$ versus z_m over the right half of the antenna, that is, $0 \leq z_m \leq h$, where $h = l/2$.
- b. Fit to the computed current samples I_m of the exact kernel to King's three-term approximation. Then, place the fitted points on the same graphs as in part (a). Discuss how well or not the three-term approximation fits the exact-kernel and the approximate-kernel current.
Repeat by using a two-term approximation. Discuss how well or not the two-term approximation fits the exact-kernel and the approximate-kernel current.
- c. To illustrate the logarithmic singularity near $z = 0$, evaluate the limiting expression at the points $z_m, m = 1, 2, \dots, M$, for $M = 200$ (the point $z_0 = 0$ is to be skipped):

$$I_{\log}(z_m) = -j \frac{4kaV_0}{\eta} \ln(k|z_m|) + \text{const.}$$

Adjust the constant so that this expression agrees with the exact-kernel current at the point z_1 , that is, $I_{\log}(z_1) = I_1$. Then, plot the imaginary parts of I_m and $I_{\log}(z_m)$ versus z_m .

- d. Repeat parts (a-c) for the antenna radius $a = 0.001$ and then for $a = 0.008$. Discuss the effect of changing the radius on the quality of the solution, both for the exact and the approximate kernel cases.
- e. Repeat parts (a-d) for the antenna length $l = 1.0\lambda$. Comment on the success of the exact versus approximate kernel calculations versus the parameters l, a, M .
- f. For each value of M and current solution $I_m, -M \leq m \leq M$, the input impedance of the antenna can be calculated from the center sample I_0 , that is, $Z_0 = V_0/I_0$. Similarly, the input admittance is:

$$Y_0 = \frac{1}{Z_0} = \frac{I_0}{V_0} = G_0 + jB_0$$

where G_0, B_0 are its real and imaginary parts, that is, the input conductance and susceptance.

For each of the values $M = 1, 2, \dots, 100$, calculate the corresponding conductance and susceptance, $G_0(M), B_0(M)$, using the exact and the approximate kernels and plot them versus M . Use the length and radius $l = 0.5\lambda$ and $a = 0.005\lambda$.

This is a time-consuming question. It requires that you solve the Hallén equation for each value of M for the exact and approximate kernels and pick the center value I_0 . Discuss the convergence properties of the exact versus the approximate kernel calculation.

25.1 Near Fields of Linear Antennas

In calculating mutual coupling effects between closely-spaced linear antennas, we need to know the fields produced by an antenna at near distances. The fields generated by a thin wire antenna with current $I(z)$ were worked out in Sec. 15.4.

We summarize these results here. All field components can be obtained from the knowledge of the z -component of the magnetic vector potential $A_z(z, \rho)$:

$$A_z(z, \rho) = \frac{\mu}{4\pi} \int_{-h}^h I(z') \frac{e^{-jkR}}{R} dz', \quad R = \sqrt{\rho^2 + (z - z')^2} \quad (25.1.1)$$

where h is the half-length of the antenna, $h = l/2$, and the geometry is shown in Fig. 25.1.1. We have used the approximate thin-wire kernel because it differs little from the exact kernel for distances $\rho > a$ (typically, when $\rho \gtrsim 5a$).

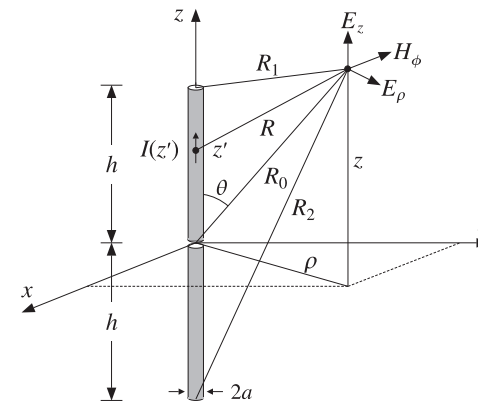


Fig. 25.1.1 Fields of a thin wire antenna.